

# Crustal structure of the French Guiana margin, West Equatorial Atlantic

C. J. Greenroyd,<sup>1</sup> C. Peirce,<sup>1</sup> M. Rodger,<sup>2</sup> A. B. Watts<sup>2</sup> and R. W. Hobbs<sup>1</sup>

<sup>1</sup>Department of Earth Sciences, University of Durham, Science Laboratories, South Road, Durham, DH1 3LE, UK. E-mail: christine.peirce@durham.ac.uk

<sup>2</sup>Department of Earth Sciences, University of Oxford, Parks Road, Oxford, OX1 3PR, UK

Accepted 2007 January 30. Received 2007 January 18; in original form 2006 September 25

## SUMMARY

Geophysical data from the Amazon Cone Experiment are used to determine the structure and evolution of the French Guiana and Northeast Brazil continental margin, and to better understand the origin and development of along-margin segmentation. A 427-km-long combined multichannel reflection and wide-angle refraction seismic profile acquired across the southern French Guiana margin is interpreted, where plate reconstructions suggest a rift-type setting.

The resulting model shows a crustal structure in which 35–37-km-thick pre-rift continental crust is thinned by a factor of 6.4 over a distance of ~70 km associated with continental break-up and the initiation and establishment of seafloor spreading. The ocean–continent boundary is a transition zone up to 45 km in width, in which the two-layered oceanic-type crustal structure develops. Although relatively thin at 3.5–5.0 km, such thin oceanic crust appears characteristic of the margin as a whole.

There is no evidence of rift-related magmatism, either as seaward-dipping sequences in the reflection data or as a high velocity region in the lower crust in the *P*-wave velocity model, and as such the margin is identified as non-volcanic in type. However, there is also no evidence of the rotated fault block and graben structures characteristic of rifted margins. Consequently, the thin oceanic crust, the rapidity of continental crustal thinning and the absence of characteristic rift-related structures leads to the conclusion that the southern French Guiana margin has instead developed in an oblique rift setting, in which transform motion also played a significant role in the evolution of the resulting crustal structure and along-margin segmentation in structural style.

**Key words:** continental margins, crustal structure, oceanic crust, seismic structure.

## 1 INTRODUCTION

Passive continental margins surround the Atlantic and demonstrate a wide variation in crustal structure. In the broadest terms, these margins can be divided on the basis of their orientation relative to the direction of plate motion at the time of break-up, into those that formed orthogonal (rifted, e.g. Hatton Bank—Morgan & Barton 1990; Galicia Bank—Whitmarsh *et al.* 1996; Namibia—Bauer *et al.* 2000; Iberia—Dean *et al.* 2000; Congo-Zaire-Angola—Contrucci *et al.* 2004; Goban Spur—Bullock & Minshull 2005; Vøring—Mjelde *et al.* 2005) and those that have developed parallel (transform, e.g. Ivory Coast—Peirce *et al.* 1996; Ghana—Edwards *et al.* 1997) (Fig. 1). In addition, oblique margins combine strike-slip movement with extension and display characteristics of both rifted and transform margins (e.g. Rio Muni and Cameroon-Guinea-Gabon—Turner *et al.* 2003; Wilson *et al.* 2003).

Fig. 1 summarizes the above examples from the East Atlantic, showing the variation in crustal structure with latitude and demonstrating differences in both the width over which the continental crust

thins and in the width of the transition zone between continental and oceanic crust. Rifted margins tend to exhibit crustal thinning over 100–400 km (Davis & Kusznir 2002) and transition zones of 10–170 km (e.g. Dean *et al.* 2000), and are often associated with faulted block structures formed during rifting (e.g. Peddy *et al.* 1989). Conversely, transform margins show more abrupt crustal thinning and a very rapid transition from continental to oceanic type crust within a zone less than 30 km in width (e.g. Edwards *et al.* 1997).

Crustal structure may also be highly influenced by the degree of rift-related magmatism, allowing further classification into two end-member types: *volcanic* and *non-volcanic*. The evolution of volcanic margins is dominated by extensive igneous activity, manifest as basaltic lava flows and imaged in multichannel seismic (MCS) reflection data as seaward-dipping reflection events (e.g. Vøring—Mutter *et al.* 1984). These margins are also characterized by magmatic underplate imaged as a high velocity region ( $>7.2 \text{ km s}^{-1}$ ) in the lower crust in wide-angle (WA) velocity–depth models. Non-volcanic margins exhibit none of these features (e.g. Iberia—Dean *et al.* 2000).

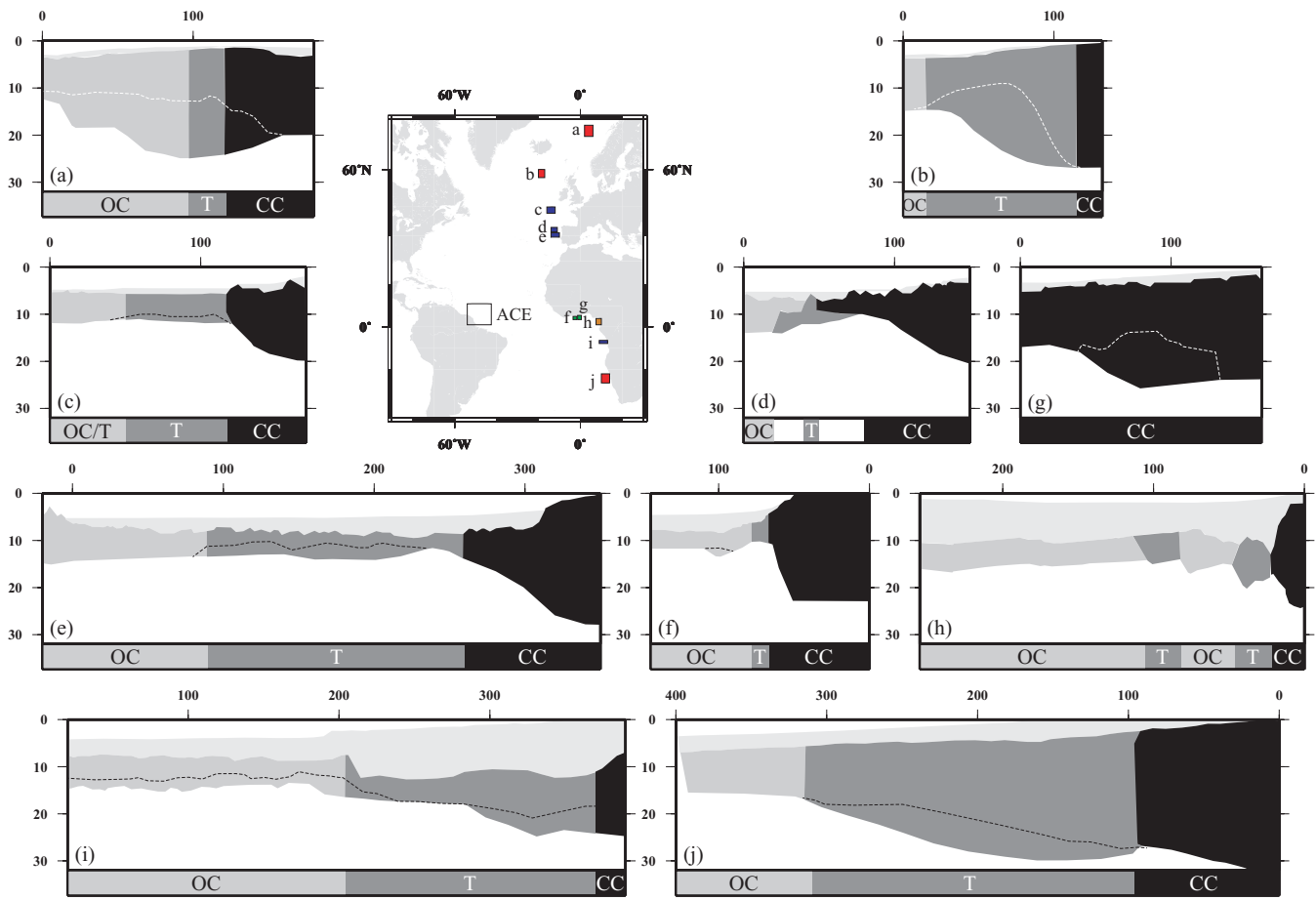


**Figure 1.** Crustal structure of the main styles of passive continental margins of the eastern Atlantic. (a) Vøring—Mjelde *et al.* 2005; (b) Hatton Bank—Morgan & Barton 1990; (c) Goban Spur—Bullock & Minshull 2005; (d) Galicia Bank—Whitmarsh *et al.* 1996; (e) Iberia—Dean *et al.* 2000; (f) Ghana—Edwards *et al.* 1997; (g) Ivory Coast—Peirce *et al.* 1996; (h) Cameroon-Guinea-Gabon—Wilson *et al.* 2003; (i) Congo-Zaire-Angola—Contrucci *et al.* 2004; and (j) Namibia—Bauer *et al.* 2000. The inset shows the geographic location of each example colour coded for margin type (red: volcanic; blue: non-volcanic; green: transform; orange: composite rift-transform characteristics). The location of the ACE study area is shown for reference (black box).

Whilst these structural styles enable broad classification of passive margins, local factors further influence their crustal structure and result in margin segmentation on many length scales. The most obvious form of segmentation is the first-order discontinuity in geometry of rifted margins resulting from transform faults, as observed on bathymetric, magnetic and gravity data from the Central Atlantic (Fig. 2). Segmentation is further evident in along-strike variation in the effective elastic thickness ( $T_e$ —e.g. Watts & Stewart 1998), rift-related magmatism (e.g. Callot & Geoffroy 2002; Wu *et al.* 2006), exhumed and serpentinized mantle (e.g. Whitmarsh *et al.* 1996), presence of thin oceanic crust (e.g. Whitmarsh *et al.* 1993) and the extent of syn- and post-rift subsidence (e.g. White & McKenzie 1989; Stewart *et al.* 2000). However, the origin of such along-strike variation is not clear and may reflect one or more of: the kinematics of break-up; the rate and duration of rifting; the underlying mantle temperature; the rate and mode of accretion of adjacent oceanic lithosphere; large-scale lateral variation in the composition and rates of erosion and flux of sediment; and the geology and physical properties of the pre-rift continental lithosphere (the inheritance).

To understand the origin and development of such along-strike variation in crustal structure, the Northeast Brazil and French Guiana margin was selected as the basis of the Amazon Cone Experiment (ACE—Watts & Peirce 2004). As part of the ACE, five

seismic margin transects were acquired (Fig. 2). Profile A was located across the southern French Guiana margin where plate reconstructions (e.g. Blarez 1986; Benkhelil *et al.* 1995—Fig. 3) suggest a rift-type setting. Profile D traverses the northeast margin of the Demerara Plateau, whose evolution gravity, bathymetry and magnetic data suggest is strongly controlled by transform continental break-up associated with the St. Paul Fracture Zone which intersects the margin at this location (Fig. 2). In addition, Profiles B, E and F were designed to image the areal variation in crustal structure and sedimentation beneath the Amazon Cone which is one of the largest deep-sea fan systems to have formed on the Earth's surface. The fan sediments act as a significant plate load and enable a flexural study of if and how lithospheric strength develops after the cessation of rifting.

In this paper we present the results of modelling seismic and gravity data acquired along Profile A, while Rodger *et al.* (2006) present the results from Profile B.

## 2 REGIONAL TECTONIC SETTING

Plate reconstructions (Blarez 1986; Nürnberg & Müller 1991; Benkhelil *et al.* 1995) show that prior to continental break-up, French Guiana and Northeast Brazil were conjugate to Guinea,

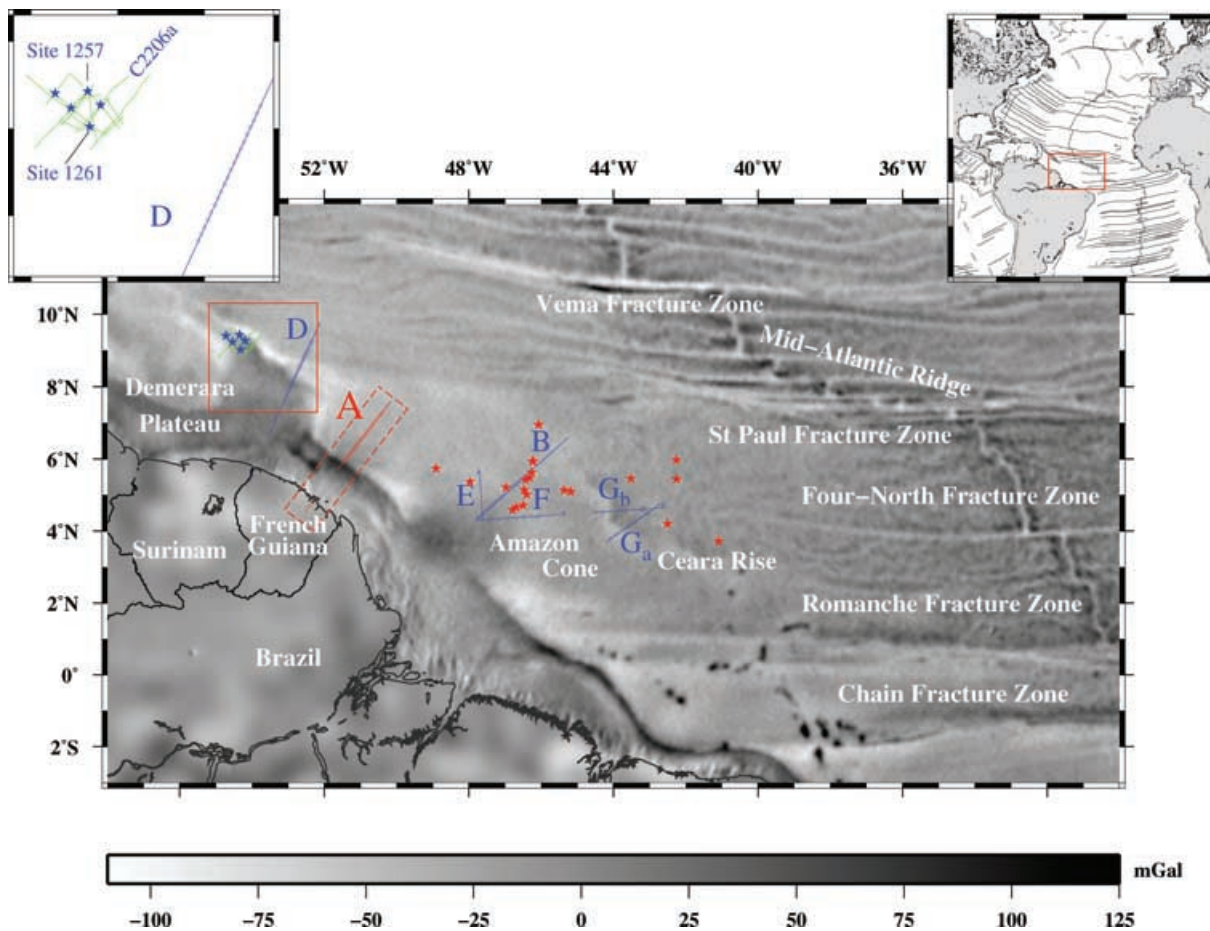


**Figure 2.** Northeast Brazil and French Guiana margin. Grey-shaded satellite-derived free-air gravity anomaly of the western equatorial Atlantic (Sandwell & Smith 1997), showing the location of large-offset transform faults at the Mid-Atlantic Ridge and their corresponding fracture zones which can be traced, in most cases, to the adjacent continental margins (inset). Also highlighted are prominent bathymetric features: the Demerara Plateau to the north; and the Amazon Cone deep-sea fan system and Ceara Rise aseismic ridge to the south. The coincident MCS and WA profile that forms the basis of this study (A) is highlighted in red, while the remaining seismic profiles (B to G) which comprise the Amazon Cone Experiment, are shown as solid blue lines with ocean-bottom instruments and land stations marked by matching circles and triangles respectively in both cases. The dashed line surrounding Profile A shows the extent of Fig. 4. Erbacher *et al.*'s (2004) seismic stratigraphic reference profiles are shown by the solid green lines, while DSDP and ODP wells are marked by red and blue stars respectively. The inset shows the location of the study area within the Atlantic and the corresponding conjugate West African margin in relation to major fracture zone traces.

Sierra Leone, Liberia, Ivory Coast and Ghana (Fig. 3). The separation of South America from Africa occurred during the early Cretaceous (~110 Ma—Nürnberg & Müller 1991). This opening is thought to have been largely accommodated by motion along the large-offset transform faults that presently offset the Mid-Atlantic Ridge (MAR). Past locations of these faults are embedded in the fabric of the seabed topography and in the gravity and magnetic fields (Fig. 2), and may be traced across the Atlantic to both its east and west margins.

Studies of the conjugate West African margin have shown that, to the north, the Liberia margin is rifted (Masche 1976), while to the south, offshore Ghana (Peirce *et al.* 1996; Edwards *et al.* 1997), the margin has transform characteristics. These along-strike structural differences are mirrored along the South American margin, implying a largely rift-type margin north of the Amazon River and a transform dominated margin to the south.

Prior to ACE, existing seismic data (confined largely to the Northeast Brazil margin) comprise shallow reflection and sonobuoy refraction profiles (Edgar & Ewing 1968; Houtz 1977; Houtz *et al.*

1977), which provide little information on lower crust and upper mantle structure. Damuth & Kumar (1975), Castro *et al.* (1978) and Braga (1991) identify an unconformity within the sediment column which they attribute to the initiation of clastic sediment deposition onto the margin from the Amazon River at ~10 Ma (Cobbold *et al.* 2004). Extrapolation of sedimentation rates from piston cores (Damuth & Kumar 1975) and the dating of cessation of pelagic sedimentation and influx of terrigenous material at Deep Sea Drilling Project (DSDP) drilling site 354 (Supko *et al.* 1977), suggest an age of 7.8–12.2 Ma (mid-late Miocene). Benjamin *et al.* (1987) conclude that the most likely source of this sediment was the uplift and erosion in the Bolivian Andes at this time, which disrupted the regional drainage pattern in the Amazon basin and diverted it from the Pacific into the Atlantic to be deposited as the Amazon Cone deep-sea fan system.

Interpretation of commercial seismic data agrees with plate reconstructions and shows that the margin started to rift during the early Cretaceous (Pereira da Siva 1989; Silva *et al.* 1999; Mello *et al.* 2001; Cobbold *et al.* 2004) with, in the Amazon region,

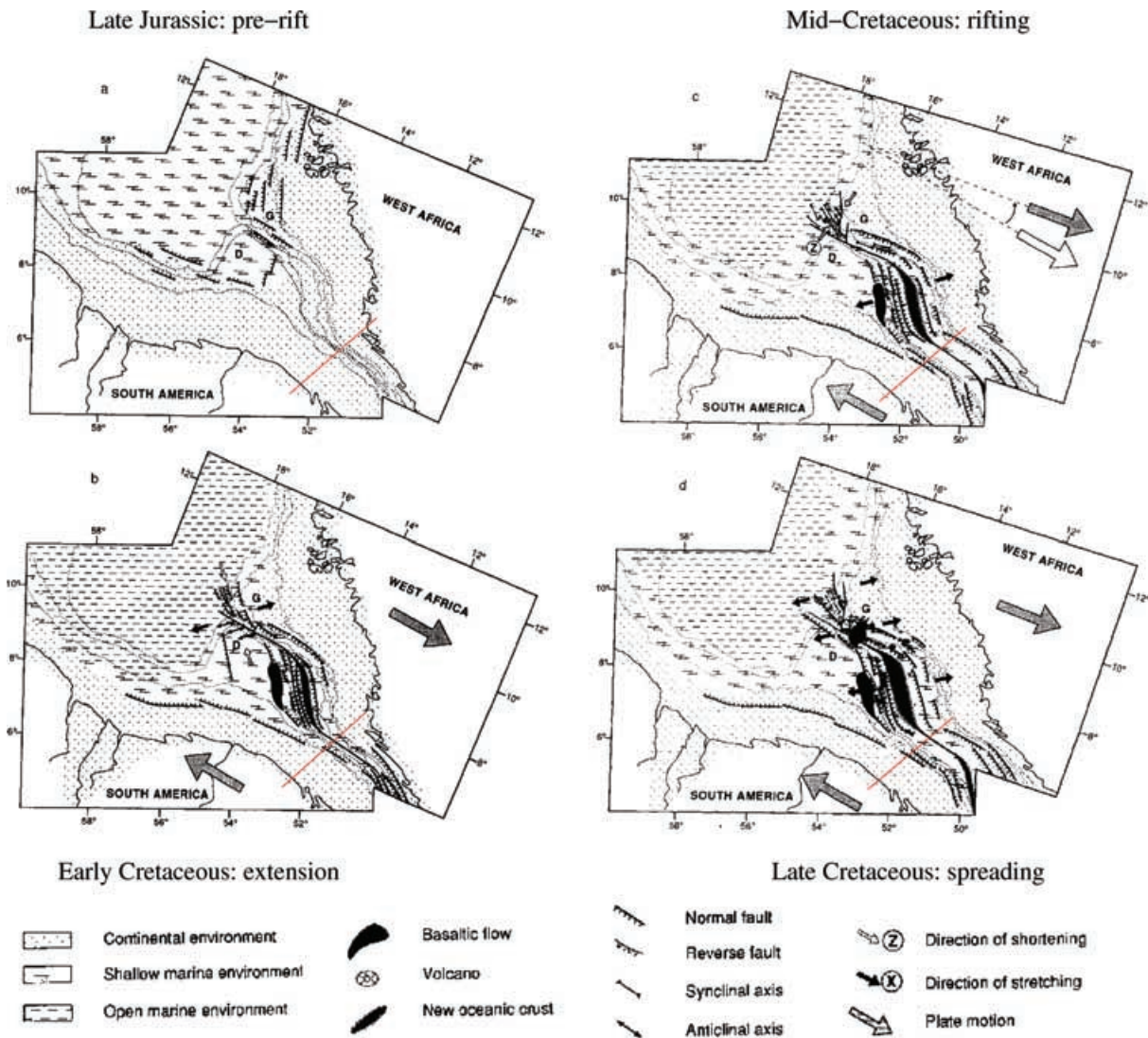


**Figure 3.** Reconstruction for the opening of the equatorial Atlantic for the Demerara Plateau and adjacent areas offshore French Guiana. The location of ACE Profile A is indicated. Benkhelil *et al.*'s (1995) model suggests that the initiation of continental break-up is a result of transensional motion between the African and South American plates during the Early Cretaceous which resulted in the inception of seafloor spreading by the early Late Cretaceous. The results of this study are consistent with this model.

rift-related structures imaged on the inner shelf, where a syn-rift, mainly coarse clastic sequence of ~100–115 Ma age is overlain by a post-rift, mainly fan-delta and platform carbonate sequence of 0–100 Ma age (Brandão & Feijó 1994). Consequently, the Amazon Cone was emplaced on the Northeast Brazil margin ~90–105 Ma after rifting ceased.

Also prior to the ACE, the only constraint on deep crustal structure along the margin as a whole was a gravity transect of the Amapa Shelf and Amazon Cone (Fig. 2). The only available constraint on densities at the time derived from velocities obtained from sonobuoy data (e.g. Houtz 1977) using a 1-D approach to data analysis. Braga (1991) modelled the Bouguer anomaly and concluded that the continental crust beneath the shelf is about 30–35 km thick and, seaward, the oceanic crust is about 10 km thick. However, this modelling could not determine the nature of the crust within the 400-km-wide region defining the ocean–continent transition (OCT), nor the role (if any) that magmatism played during rifting.

Further north at the French Guiana margin, existing seismic data are limited to industry MCS and well data (Gouyet *et al.* 1993) and

site survey and borehole data from Ocean Drilling Program (ODP) sites 1257 to 1261 (Erbacher *et al.* 2004), acquired between 8.5°N and 9.5°N, 53.5°W and 55°W on the Demerara Plateau (Fig. 2). These data will be used as the primary stratigraphic reference for the sediment column for this study.

### 3 THE DATA SET

The data set collected in November 2003 onboard the *RRS Discovery*, consists of six MCS reflection profiles, totalling over 2100 km in length (Fig. 2). Ocean-bottom seismographs and hydrophones (OBS/Hs) were deployed along five of these profiles, with additional land stations on two of these profiles (A & D). Underway bathymetry, gravity and magnetic data were acquired along each profile. The Global Positioning System (GPS) was used as the navigational reference and time standard for all seismic acquisition. Profile A (Fig. 4) comprises coincident 265-km-long MCS and 427-km-long WA seismic, gravity and magnetic profiles.

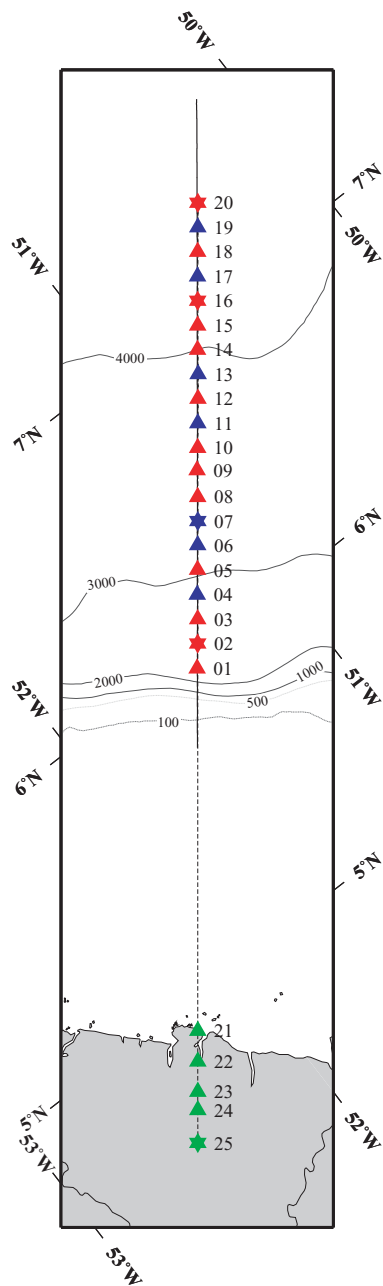


**Figure 4.** Acquisition geometry for Profile A with the seismic shot locations marked by the solid black line. OBS locations are shown as red, OBH locations as blue and land stations as green triangles respectively. The dashed line shows the full extent of Profile A, traversing ~470 km across the French Guiana margin. Example record sections from a subset of these instruments (marked by stars instead of triangles) are shown in Figs 8–12. Bathymetric contours are shown every 1000 m (solid), together with the 100 m (dashed) and 500 m (dotted) contours to highlight the location of the continental slope and rise.

### 3.1 Regional stratigraphy

We have used industry MCS and borehole data from ODP sites 1257 to 1261 (Gouyet *et al.* 1993; Silva *et al.* 1999; Erbacher *et al.* 2004) to provide the stratigraphic reference for the sediment column imaged within the region and, in particular, along Profile A (Fig. 5). Silva *et al.* (1999) observe that, within the Amazon Cone, mid-late Miocene–Recent sediments are characterized by low

amplitude, discontinuous seismic facies. In contrast, the underlying Palaeocene–mid-Miocene sediments are identified as continuous, parallel, high-amplitude facies. Only a thin veneer of the Miocene–Recent sediments is observed by Erbacher *et al.* (2004) over the Demerara Plateau. Furthermore, they show that the sediment column may be characterized by five key MCS reflectors (O, A, B, B' and C) which divide the seismic stratigraphy into four major units (1–4). Erbacher *et al.* (2004) use the five ODP borehole logs to correlate this seismic stratigraphy with lithology (Fig. 5) as follows.

Directly beneath the seafloor, Unit 1 is identified as semi-lithified sediment (primarily Miocene–Pliocene nannofossil ooze), which thins seawards. Seismically, the unit consists of a well-defined set of coherent reflection events of varying amplitude with a bright reflection event capping a seismically incoherent zone in the lowest 50 ms of the unit.

Reflector A is presumed to be a lower Miocene erosional unconformity which separates Unit 1 from Unit 2, a mainly Eocene–early Miocene nannofossil chalk sequence with Reflector B at its base. Unit 2 ranges in ‘thickness’ at the ODP sites, from 160 to 495 ms two-way traveltime (TWTT). The unit shows incoherent reflection characteristics which Erbacher *et al.* (2004) interpret as either a disturbed sediment package or the effect of side echoes from local topography.

Reflector B marks the top of Unit 3 and is hummocky on a local scale, most likely cut by channels. The uppermost section of Unit 3, named Unit 3a, contains several high-amplitude reflection events overlying a transparent zone to the top of Reflector B'. The unit appears flat lying and ranges from 40 to 160 ms ‘thick’ between the boreholes. Reflector B' lies within Unit 3 and represents the top of a black shale sequence. The presence of Type II kerogen within the shale indicates a marine source for the organic matter.

Reflector C is defined as the base of the black shale sequence. Underlying Unit 4 consists of Albian-age claystone, clayey siltstone and sandstone. At Site 1257 the Unit 4 reflectors appear folded into a low amplitude anticline, which intersects with Reflector C as an angular unconformity.

Dating of borehole cores suggests that sedimentation rates have varied during the last ~110 Myr. In the late Cretaceous deposition occurred at 3–9 m Myr<sup>-1</sup>, increasing markedly across the K–T boundary to 7–15 m Myr<sup>-1</sup> during the Palaeocene to mid-Eocene, with deposition rates having a pronounced 20–50 kyr periodicity. Recent sediments are generally too thin to obtain a good estimate of sedimentation rate. However, at site 1261 sedimentation rates of up to 65 m Myr<sup>-1</sup> in the late Miocene–early Pliocene are observed.

### 3.2 Multichannel seismic data

As part of the ACE, MCS data were acquired using a 2.4 km, 96-channel streamer with shots fired by an array of 14 airguns of various chamber sizes totalling 6520 in<sup>3</sup> (~107 l) in volume. The array was of a compromise design, producing a high energy, relatively low frequency source signature for deep crustal WA seismic data acquisition, whilst also being compatible with contemporaneous MCS imaging. Shots were fired at 40 s intervals which, at a surveying speed of ~4.85 kn, results in an average shot interval of ~100 m. Data were recorded for 20 s after each shot and at a sampling interval of 4 ms. Processing was undertaken using ProMAX, with a simple processing flow (which included velocity analysis, stacking, multiple removal/suppression and time migration) giving the best results. The processed MCS data image the entire sediment column,

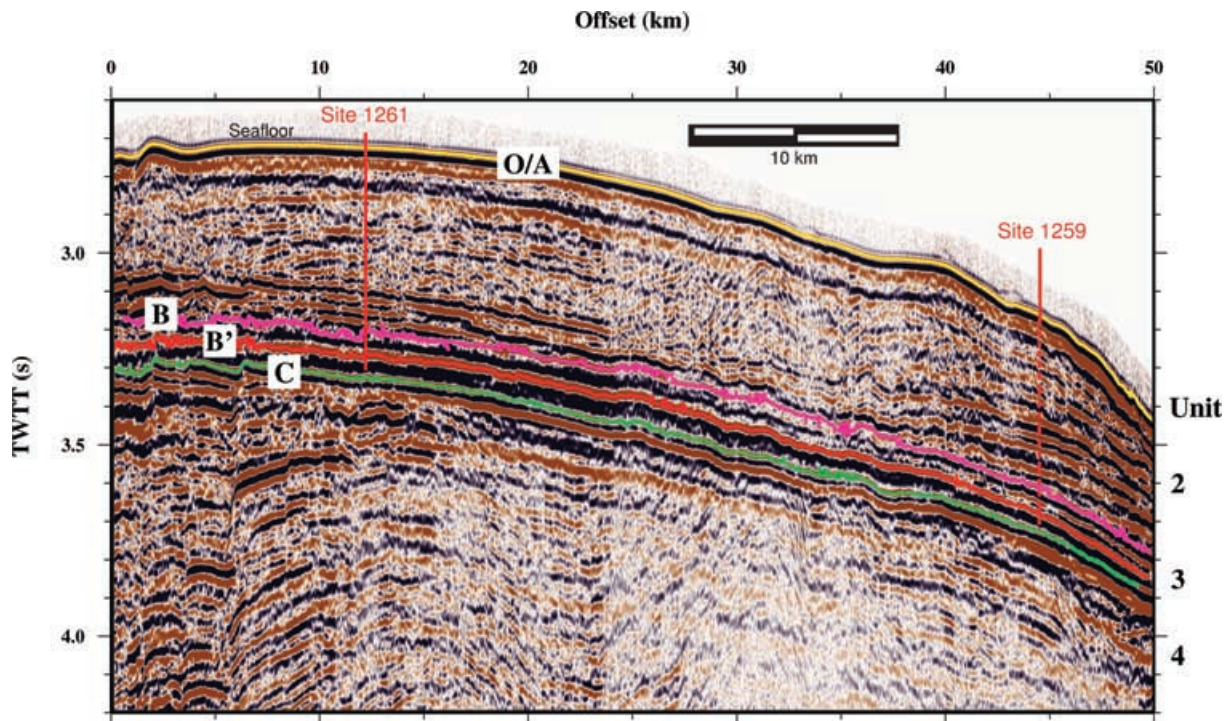


**Figure 5.** Regional seismic stratigraphic reference line C2206a of Erbacher *et al.* (2004), developed from MCS data acquired as part of commercial and ODP site survey studies. See text for details;

from a relatively smooth seafloor down to the top of the basement (Fig. 6).

A 3.5 to 4.5 s TWTT sedimentary zone is identified from stratified reflectors with interval velocities ranging from 1.6 to 3.5 km s<sup>-1</sup> (Fig. 6). The interval velocity gradient within the top kilometre below seafloor ( $\sim 0.8$  s<sup>-1</sup>) is relatively steep, suggesting a rapidly compacting upper unit overlying a lower unit of lower gradient ( $\sim 0.25$  s<sup>-1</sup>).

Several sedimentary packages are identified in Fig. 6, each separated by a clear reflection event, which can often be traced across the whole profile. A significant high amplitude reflection event at  $\sim 7.5$  s TWTT is interpreted as an unconformity (labelled MM in Fig. 6), separating subparallel reflectors below from those onlapping above. This unconformity shows similar characteristics to another identified within the sedimentary stratigraphy of the Amazon Cone to the south (Silva *et al.* 1999; Rodger *et al.* 2006), which has been dated as mid-Miocene in age (Damuth & Kumar 1975; Braga 1991). The latter unconformity separates shallow late-Miocene, Pliocene and Quaternary sediments above from deeper Cretaceous to early-Miocene sediments below, and which Braga (1991) used to date the onset of the fan deposition. There is little evidence of post-rift faulting within the sediments further offshore. However, heading landwards as the slope increases towards the continental shelf, we interpret the complex patterns of reflection events as evidence of significant slumping along large faults (Fig. 7). The hummocky nature of the basement reflection beneath the deepest sediments suggests that the underlying crust is oceanic and, consequently, that all sediments imaged are post-rift.

The sediments above the mid-Miocene unconformity were subdivided into three units for inclusion in the main WA seismic model, based on the strongest, most continuous reflectors. Two further units were identified beneath the unconformity. A clear basement reflection is observed heading landwards to  $\sim 240$  km, at which point it

becomes obscured by the seafloor multiple (Fig. 6). There is no evidence of any reflectors (e.g. Moho) beneath the basement reflector. There is also no evidence for tilted basement fault blocks, commonly observed at rifted continental margins (e.g. Goban Spur—Peddy *et al.* 1989) nor seaward-dipping reflector (SDR) sequences often associated with volcanic margins.

### 3.3. Marine wide-angle refraction data

Twenty OBS/Hs were deployed along Profile A (Fig. 4). All instruments were equipped with hydrophones and additionally, 13 were fitted with three-component 4.5 Hz geophone packages. Instruments were deployed at 10 km intervals from the base of the continental slope, across the rise and out into the abyssal plain. All instruments were successfully recovered, however OBS 8 failed to record any usable data.

Direct water waves ( $W_w$ ) and crustal diving rays ( $P_s$  and  $P_g$ ) are observed as first arrivals on all WA record sections (Figs 8–11). In addition, mantle ( $P_n$ ) diving rays are also recorded by OBS/Hs deployed at the seaward end of the profile. Secondary phases are observed and identified as intra-sediment and intra-crustal arrivals, intra-crustal reflections ( $P_gP$ ) and Moho reflections ( $P_mP$ ). The sediment arrivals are subdivided into five types ( $P_{s1}$  to  $P_{s5}$ ) to be consistent with the MCS data, and crustal arrivals into two types ( $P_{g1}$  to  $P_{g2}$ ) to accommodate the major changes in velocity observed on the record sections, and to be compatible with the standard models of oceanic and continental crustal structure (e.g. Spudich & Orcutt 1980; Bratt & Purdy 1984; Christensen & Mooney 1995). Seabed and intra-crustal multiples are also observed.

In general, the OBS/H data show clear sedimentary and upper basement (1.7 to 4.5 km s<sup>-1</sup>) first arrivals emerging from the direct water wave, out to source-receiver offsets of  $\sim 15$  km. Mid-lower crustal ( $\sim 6$  km s<sup>-1</sup>) and uppermost mantle ( $\sim 8$  km s<sup>-1</sup>) arrivals are

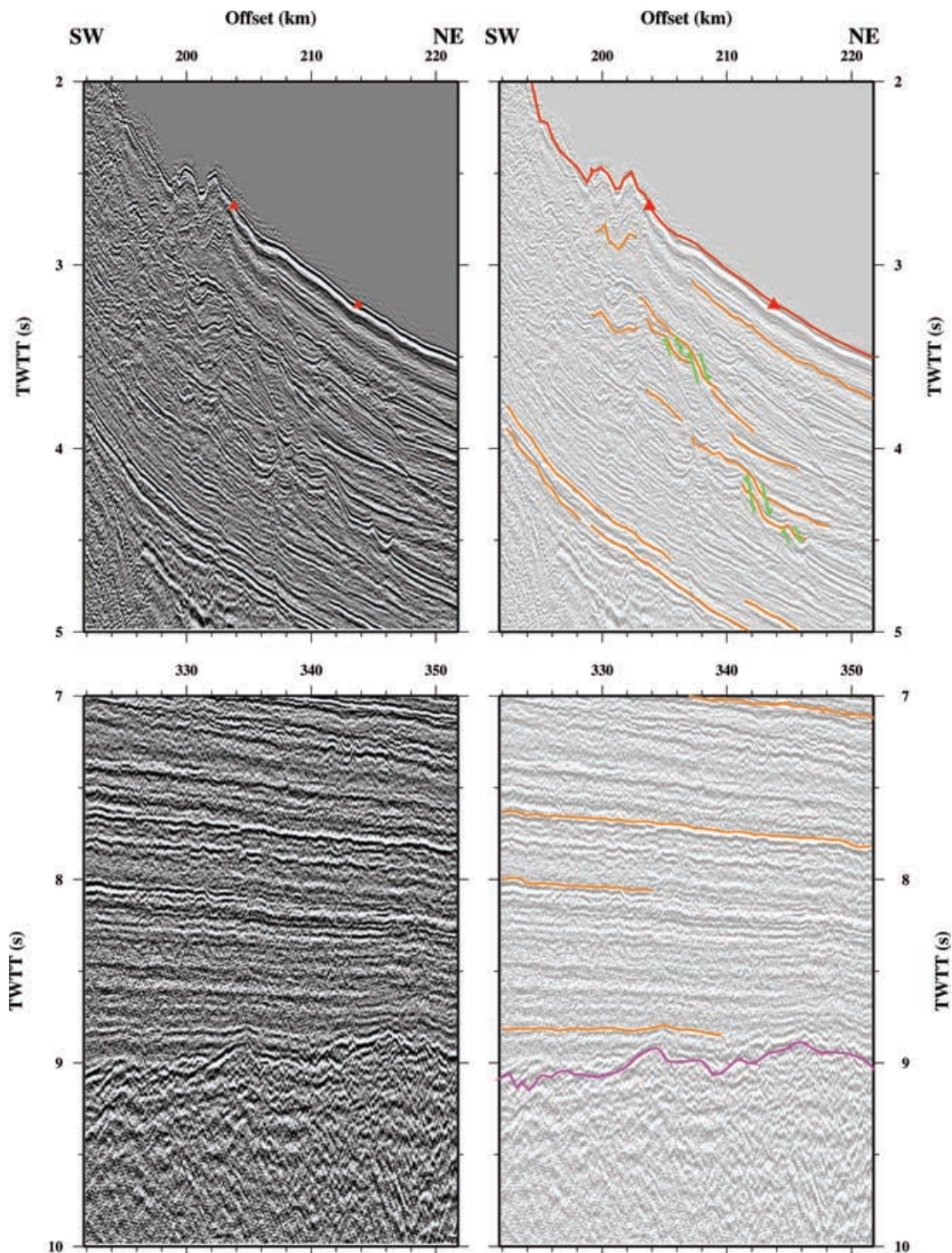


**Figure 7.** Enlarged view of features imaged in the MCS data from Profile A. Top: Slumping along large faults. Bottom: Basement surface (purple) with overlying Cretaceous to early-Miocene sediments. The oceanic crustal basement surface is characterized by high amplitude irregular, hummocky reflection events.

observed at offsets up to  $\sim 200$  km from the instrument. Four example record sections for instruments 2, 7, 16 and 20 are shown in Figs 8–11, and show features characteristic of all other sections. The main characteristics of each example section are briefly described below.

OBS 20 is located at the seaward end of the profile (Fig. 8) and its record section shows relatively symmetrical arrivals either side of the instrument position. Sedimentary first arrivals ( $P_s$ ) are recorded

at source-receiver offsets of  $\sim 7$ – $15$  km, with  $P$ -wave velocities no greater than  $\sim 3$  km s $^{-1}$ . A clear secondary arrival, however, indicates higher velocities  $> 3.5$  km s $^{-1}$ . For the crust, low amplitude first arrivals ( $P_g$ ) are observed at  $\sim 15$ – $23$  km offset at velocities in excess of  $6$  km s $^{-1}$  and, to offsets of  $\sim 60$  km, upper mantle ( $P_n$ ) diving rays at velocities  $\sim 8$  km s $^{-1}$ . The large amplitude Moho reflection ( $P_mP$ ) at offsets greater than  $\sim 23$  km constrains the total crustal thickness at between  $8$  and  $10$  km. These velocities are

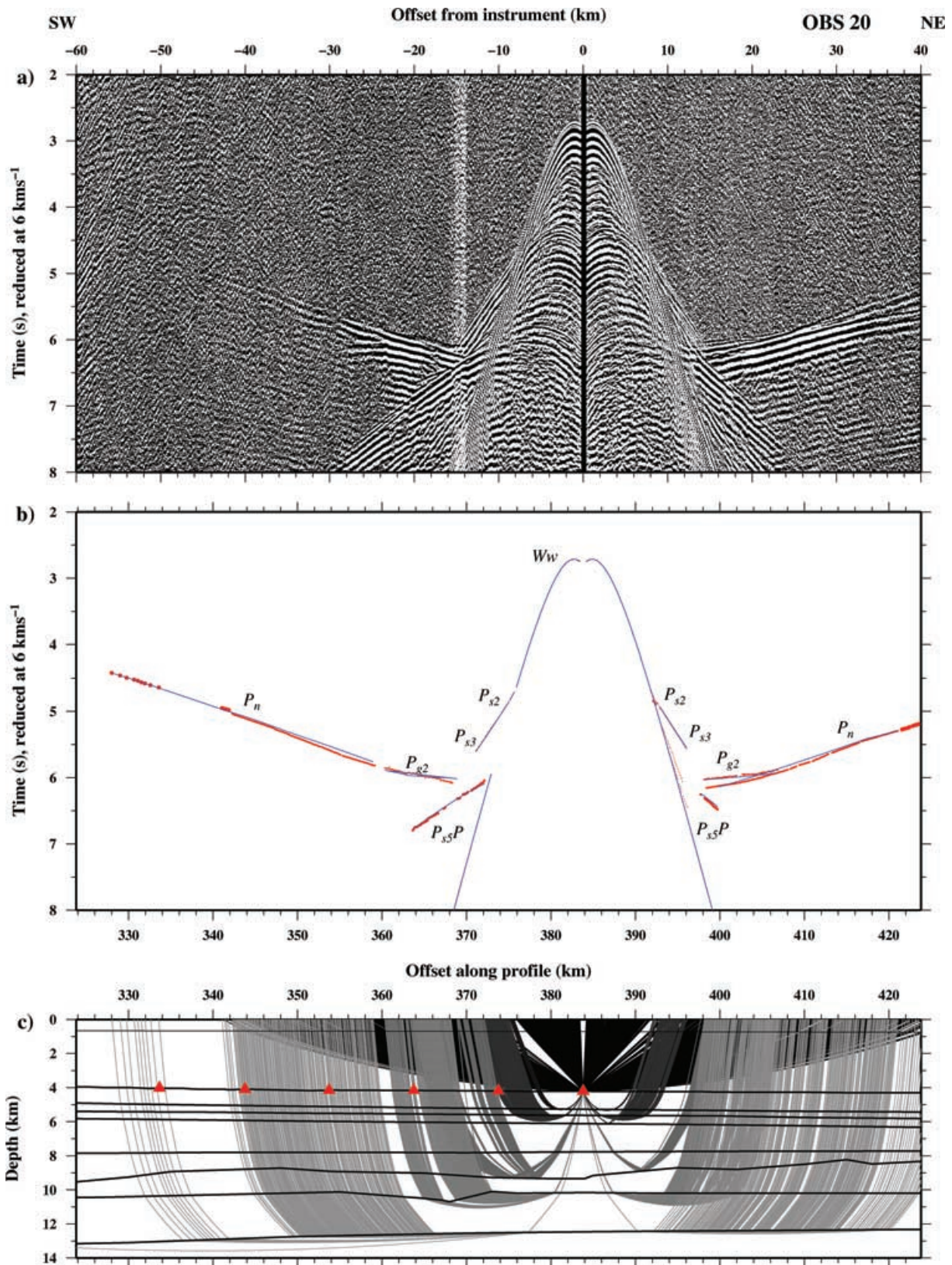


**Figure 8.** Ray-trace modelling of hydrophone data recorded by OBS 20 located towards the base of the continental slope (see Fig. 4 for instrument location). (a) Filtered record section plotted at true amplitude. The horizontal axis shows offset from the instrument position. (b) Record section showing observed (red vertical bars whose length represents the assigned picking error) and calculated (blue lines) traveltime picks for comparison with the observed data shown in (a). For this, and the ray diagram in (c), the horizontal axis shows offset along Profile A. (c) Ray diagram showing modelled arrivals. The complete final model, including velocity annotation, is shown in Fig. 13. Red triangles show OBS locations. Both record sections are plotted at a reduction velocity of  $6 \text{ km s}^{-1}$  and are plotted at the same horizontal scale with each part aligned to the instrument position. Arrival labels are defined in the text.

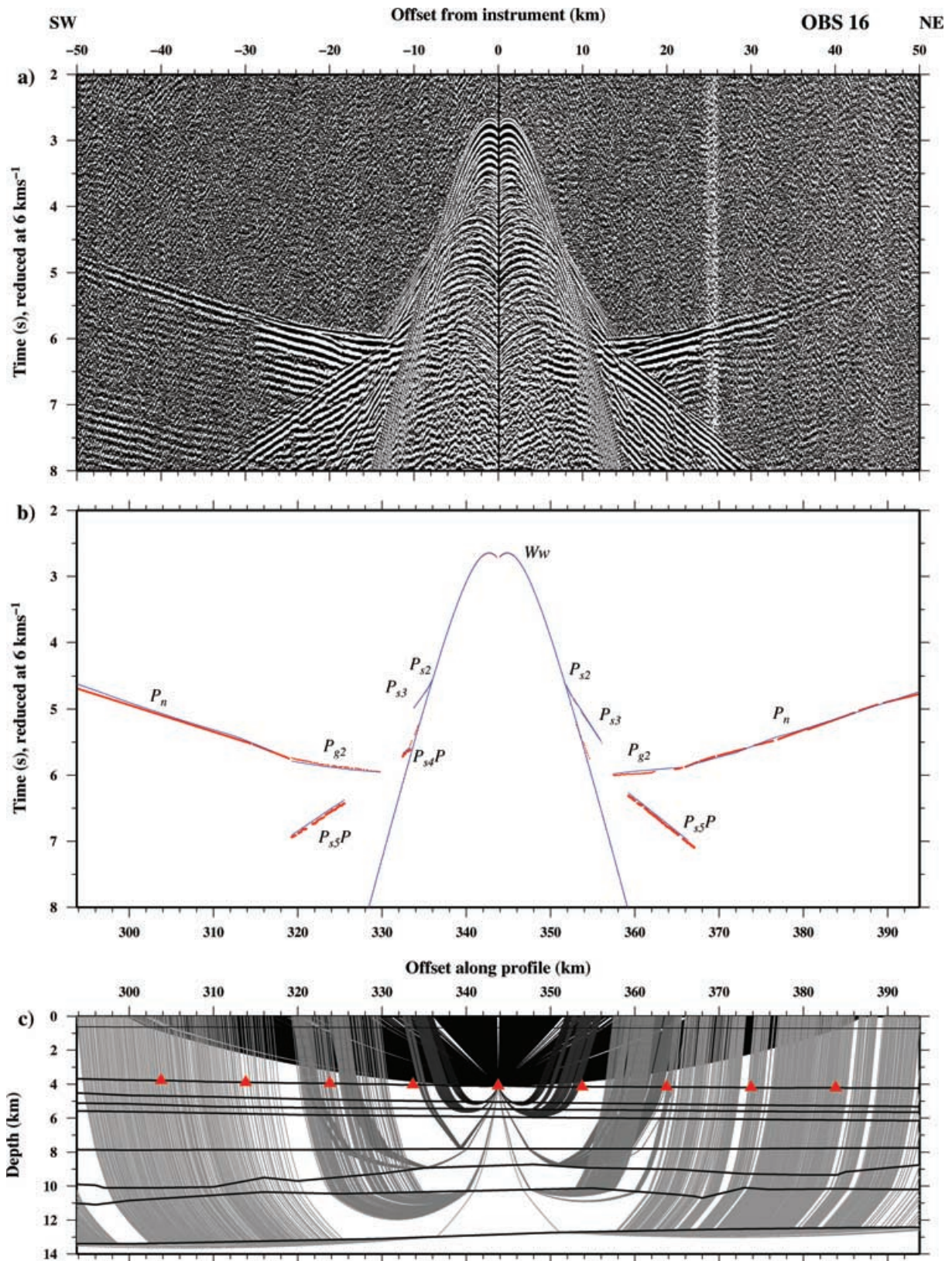


Figure 9. Ray-trace modelling of hydrophone data recorded by OBS 16 (see Fig. 4 for instrument location). See Fig. 8 for details.

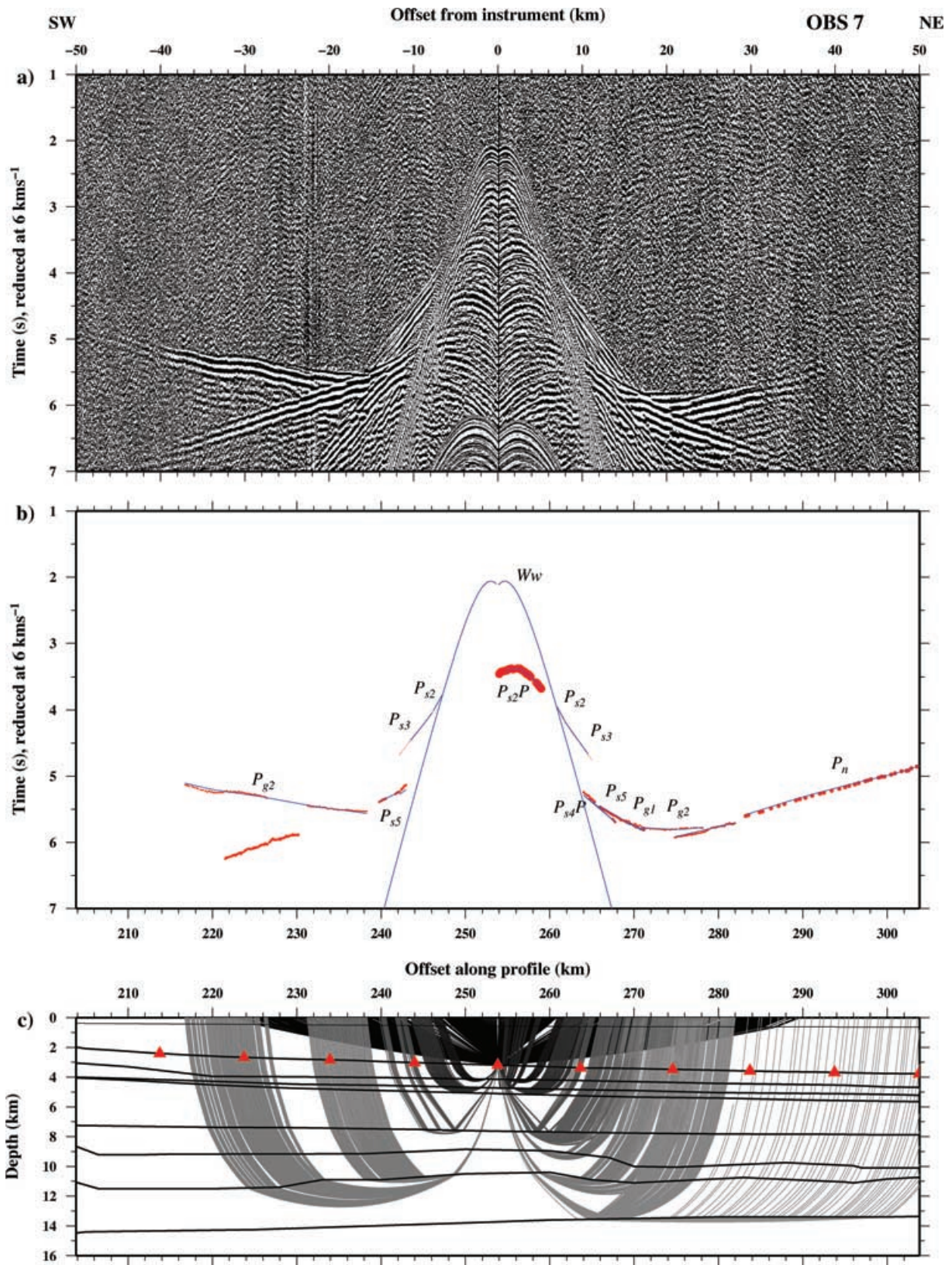


Figure 10. Ray-trace modelling of hydrophone data recorded by OBS 7 (see Fig. 4 for instrument location). See Fig. 8 for details.

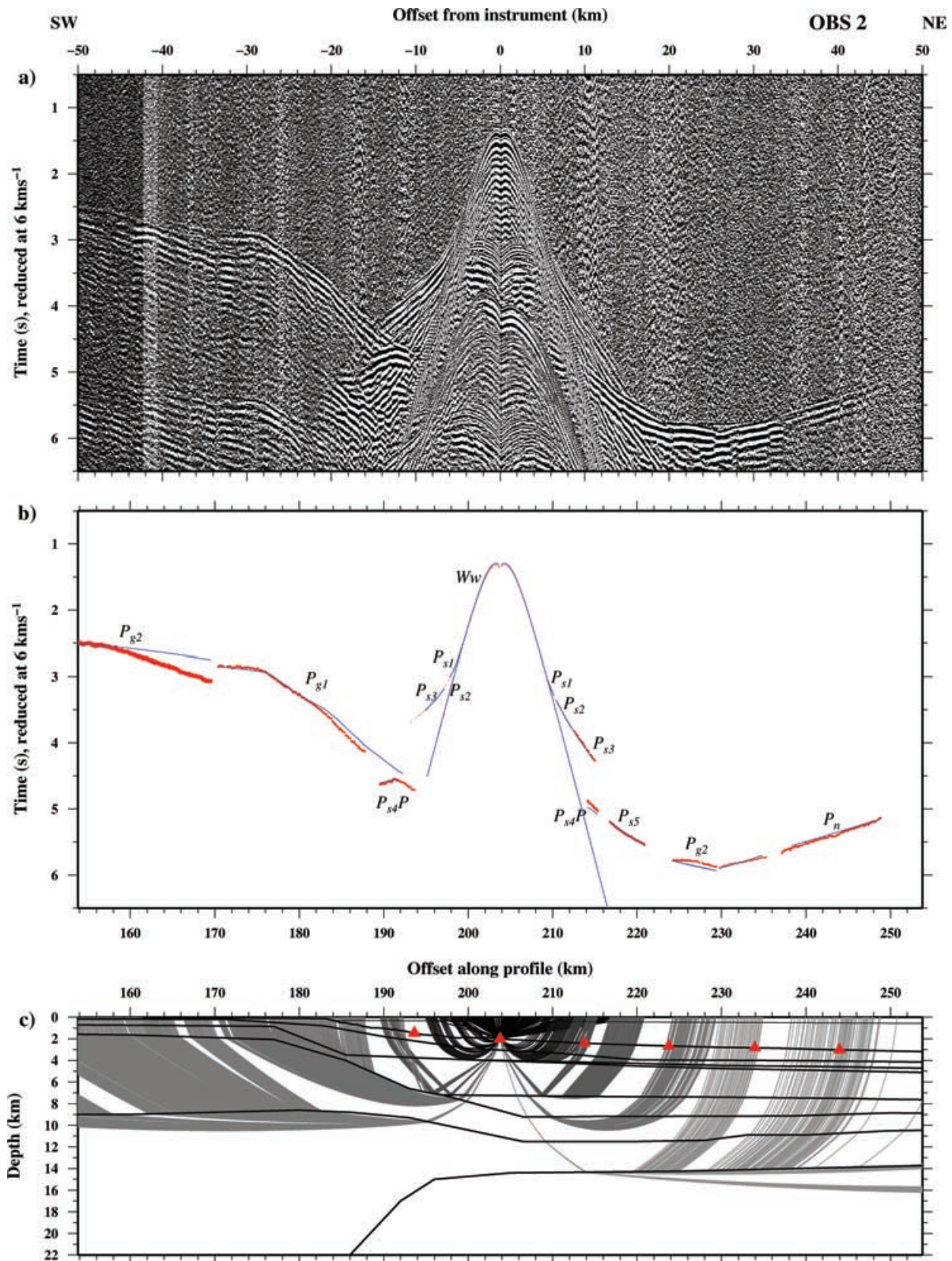


Figure 11. Ray-trace modelling of hydrophone data recorded by OBS 2 (see Fig. 4 for instrument location). See Fig. 8 for details.

consistent with normal oceanic crust overlying typical upper mantle (e.g. White *et al.* 1992) at the most seaward end of the profile.

OBS 16 (Fig. 9) shows a similar pattern to OBS 20. On this and adjacent instruments,  $P_n$  arrivals on the seaward side appear to be of a higher relative amplitude, and are observed to offsets of  $\sim 110$  km.

OBS 7 (Fig. 10) shows a degree of asymmetry, largely related to the onset of rapid shallowing of the seabed. However, at this instrument  $P_n$  arrivals are not observed from landward shots, which may also reflect a corresponding thickening of the crust. Record sections from instruments located landwards of OBS 7 show a significant degree

of asymmetry with, for example, crustal arrivals landward of the instrument location arriving up to 3 s earlier than at equivalent offsets seaward (see OBS 2—Fig. 11). This asymmetry suggests a major structural change within the crust. There are several possibilities which may not be mutually exclusive:

- (a) a significant increase in thickness of the sediment column is observed on the MCS data;
- (b) the seabed rapidly shallows on the continental rise and slope and
- (c) crustal thickness should increase landwards associated with the OCT.

### 3.4 Land wide-angle refraction data

Five SEIS-UK 6TD land seismographs were deployed to record the marine shots at large offset. This onshore extension of the profile was designed to image the thickness and structure of the pre-rift crust and provide control on the lower crustal structure in the region beneath the shelf/rise where it changes most rapidly adjacent to the OCT. The instruments were deployed between Cayenne and Cacao in French Guiana (Fig. 4), and were all located within 47 km of the coastline. The furthest instrument inland was located ~160 km from the most landward shot. All instruments recorded a similar pattern of arrivals and an example data section from land station 25 (Fig. 4) is shown in Fig. 12. Using a reduction velocity of  $8 \text{ km s}^{-1}$  to highlight lower crust and upper mantle phases, the first arrivals dip gradually with a velocity of  $\sim 6 \text{ km s}^{-1}$  and are identified as  $P_g$  phases. A clear  $P_mP$  arrival is observed at  $\sim 8 \text{ s}$  traveltime between  $\sim 130$  and  $190 \text{ km}$  offset, together with an upper mantle  $P_n$  arrival of velocity  $\sim 8 \text{ km s}^{-1}$ . The transition between these phases is complicated by the lateral variation in sediment thickness coupled with the variation in seabed depth beneath the corresponding shots.

## 4 SEISMIC MODELLING

A  $P$ -wave velocity–depth model of the crust was constructed by forward modelling the WA seismic data using the MCS data to provide constraint on the layering within the sediment column and the depth to basement. Traveltime picking followed the approach outlined by Zelt (1999) with an error of  $\pm 15 \text{ ms}$  ( $\sim 4$  samples) assigned to near-offset first arrivals and between  $\pm 20$  and  $100 \text{ ms}$  for longer offset arrivals depending on the signal-to-noise ratio. Secondary arrivals often had their onset masked by preceding arrivals. Consequently, the error was increased by  $\pm 40 \text{ ms}$  (about half a wavelength). The land station data were assigned larger errors ( $\pm 100$  to  $200 \text{ ms}$ ) due to difficulties in arrival identification, the lack of a clear first break and an increase in the level of background noise.

### 4.1 Forward modelling

Forward traveltime modelling was undertaken using *RAYINV*R (Zelt & Smith, 1992), adopting a strategy closely resembling that of Zelt (1999) in which a starting model was created using a simplistic 1-D interpretation of first arrival data for each instrument draped beneath the seafloor. The main sedimentary layers and basement surface were incorporated from the MCS data interpretation, converting the TWTs of interfaces to depth using the processing-based interval velocities.

Examples of the ray-trace modelling are shown for OBS 2, 7, 16, 20 and land station 25 in Figs 8–12. The fit of the final model to

**Table 1.** Number of traveltime picks ( $n$ ), misfit between calculated and picked traveltime ( $m_{rms}$ ) and normalized  $\chi^2$  for each identified phase.

Phase	$n$	$m_{rms}$ (ms)	$\chi^2$
$W_w$	9021	14	0.84
$P_{s1}$	85	11	0.57
$P_{s2}$	386	16	1.19
$P_{s3}$	795	14	0.85
$P_{s4}$	0	-	-
$P_{s5}$	650	27	1.00
$P_{s2}P$	46	47	0.87
$P_{s3}P$	26	20	0.17
$P_{s4}P$	554	43	0.58
$P_{s5}P$	917	32	0.31
$P_{g1}$	435	61	1.68
$P_{g2}$	3194	54	1.07
$P_{g1}P$	0	-	-
$P_n$	3586	73	1.11
$P_mP$	398	44	0.79
All OBS phases	20093	42	0.92
$P_{g2}$	962	115	1.07
$P_mP$	519	144	1.87
All land station phases	1481	126	1.35

all observed data within the pick errors was assessed using misfits and  $\chi^2$  values (Zelt 1999) analysed instrument by instrument, layer by layer across the whole profile (Table 1). The best-fit, preferred model (Fig. 13) is  $427 \text{ km}$  in length with land instruments located between  $0$  and  $45 \text{ km}$  model offset and OBS/Hs between  $193$  and  $383 \text{ km}$  offset. Shots were fired between  $117$  and  $425 \text{ km}$  model offset.

## 4.2 Results

The best-fit  $P$ -wave velocity model is defined by the water column (identified as *Water* on Fig. 13), five sediment layers (*Sediments*), the basement crust and the upper mantle (identified as *Mantle*). The basement crust is further divided into two layers termed *Layer 2* and *Layer 3* to reflect the oceanic-type crust expected at the seaward end of the profile, and *Upper Crust* and *Lower Crust* for the continental-type crust expected at the landward end of the profile. A comparison of layer boundaries which define the  $P$ -wave velocity model with reflectors picked from the MCS data is shown in Fig. 6.

The model can be broadly divided into (Fig. 13):

- (i) sediment column ( $180$ – $430 \text{ km}$  model offset);
- (ii) continental crust ( $0$ – $135 \text{ km}$ );
- (iii) thinned continental crust ( $135$ – $206 \text{ km}$ );
- (iv) the transition zone ( $206$ – $250 \text{ km}$ ) and
- (v) oceanic crust ( $250$ – $430 \text{ km}$ ).

The characteristics of each of these are discussed below and a summary of layer  $P$ -wave velocities and thicknesses is contained in Table 2. Quantitative analysis of the resolution of the model and the goodness of fit to the observed data is summarized in Table 1.

### 4.3.1 Sediment column

Beneath the seabed, the  $P$ -wave velocity model comprises five sedimentary layers within the *Sediment* unit—termed *S1*–*S5*. Within this unit the  $P$ -wave velocity increases from  $1.62 \text{ km s}^{-1}$  immediately beneath the seafloor to  $\sim 4.7 \text{ km s}^{-1}$  at the base of the sediment column, following a velocity–depth profile and velocity gradients typical of

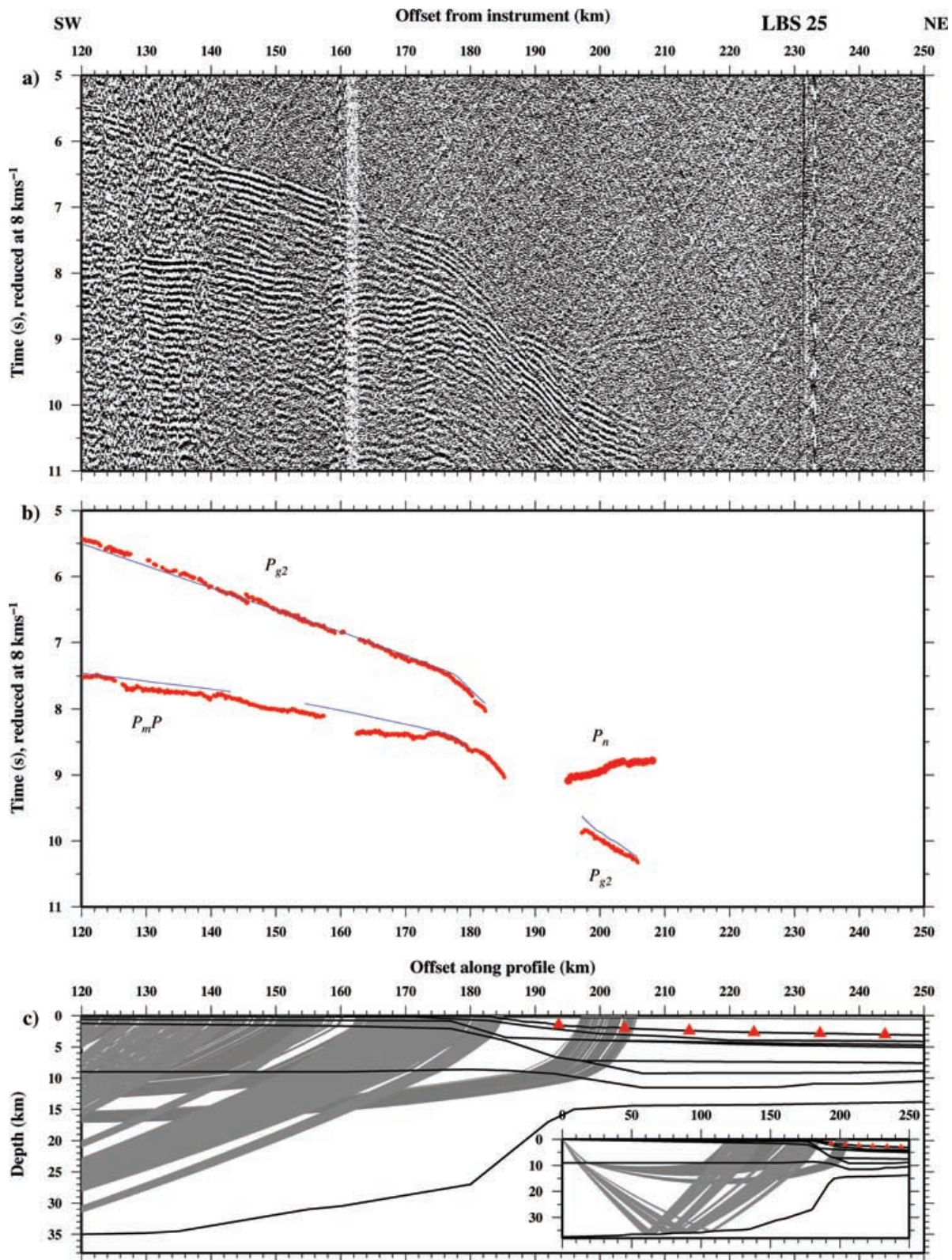


**Figure 12.** Ray-trace modelling of vertical geophone data recorded by land station 25 located at the southwest end of Profile A (see Fig. 4 for instrument location). (a) Filtered record section plotted at true amplitude. The horizontal axis shows offset from the instrument position. Arrival labels are defined in the text. (b) Record section showing observed (red vertical bars whose length represents the assigned picking error) and calculated (blue lines) traveltime picks for comparison with the observed data shown in (a). For this, and the ray diagram in (c), the horizontal axis shows offset along Profile A. (c) Ray diagram showing modelled arrivals. The complete final model, including velocity annotation, is shown in Fig. 13. Red triangles show OBS locations. Inset shows the location of the five land stations (red triangles) at the southwest end of Profile A relative to the modelled arrivals. Both record sections are plotted at a reduction velocity of 8 km s<sup>-1</sup> and are plotted at the same horizontal scale with each part aligned to the instrument position.

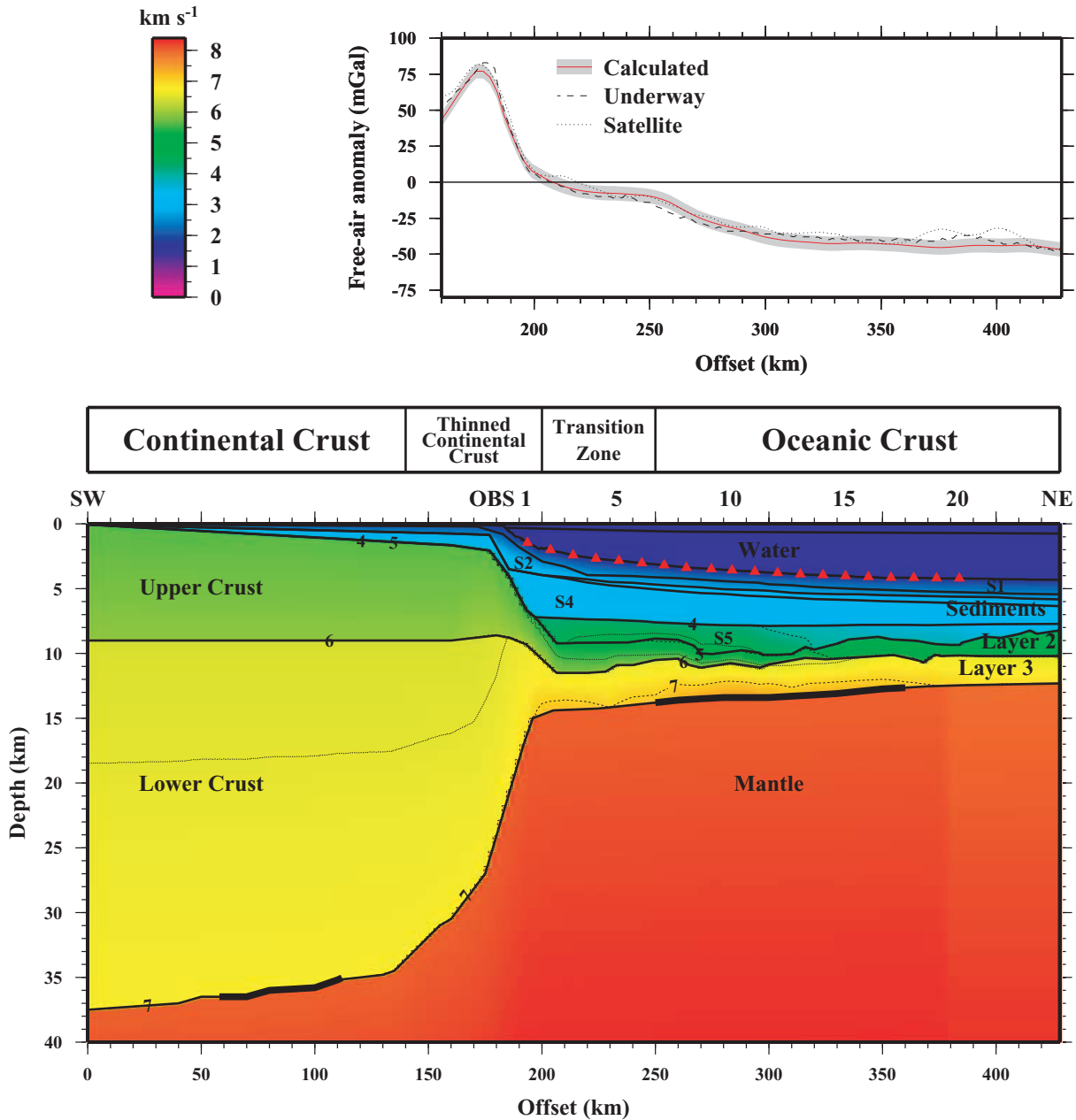


**Figure 13.** *P*-wave velocity model (bottom) of the French Guiana margin. A simplified illustration of the interpreted crustal units is also shown (middle). Velocities are colour-coded and contours annotated in  $\text{km s}^{-1}$ . Red triangles mark OBS/H locations (see Fig. 3). *S1*–*S5* are sedimentary layers. *Layer 2* and *Layer 3* refer to interpreted oceanic crust, while the continental crust is divided into *Upper Crust* and *Lower Crust* layers. In both cases the  $6 \text{ km s}^{-1}$  iso-velocity contour marks the transition between the two crustal layers. Crustal ages and fracture zone traces (after Müller *et al.* 1997) are annotated. *P*-wave velocities were converted into density as outlined in the text and the free-air gravity anomaly calculated (solid red line) for comparison (top) with that acquired whilst seismic surveying (dashed). The satellite-derived (Sandwell & Smith 1997), longer-wavelength anomaly is included (dotted). Densities—in  $\text{g cm}^{-3}$ —are annotated for each layer in the model and summarized in Table 2.

oceanic *Layer 1* (Fig. 14; White *et al.* 1992). The conversion of the final WA model into TWTT (Fig. 6) demonstrates the consistency between sedimentary layer boundaries and the prominent events in the reflection data.

A major unconformity at  $\sim 7.5 \text{ s}$  TWTT (Fig. 6) separates the upper sediments (*S1*–*S3*) from those below (*S4*–*S5*) and is associated with a large change in velocity gradient ( $0.65$ – $0.30 \text{ s}^{-1}$ ) (Figs 13 and 14). Few refracted arrivals are observed from the lower sedimentary layers and the final model shows significant lateral thinning and velocity decrease oceanwards. The velocity gradient in these layers

( $0.30 \text{ s}^{-1}$ ) is consistent with the very low interval velocity gradient immediately below the unconformity derived from the MCS data, which in turn increases with depth (Fig. 6).

The base of the *Sediment* column is primarily constrained by a combination of refractions ( $P_g$ ) and reflections ( $P_gP$ ), to be a smooth surface (within the resolution of the WA data at that depth) with up to  $\sim 2 \text{ km}$  of topography along the entire profile. However, the MCS data (Figs 6 and 7 and depth converted using the WA velocity model) reveals that the basement surface is in fact quite hummocky, particularly so seawards of the continental rise, and underlies

**Table 2.** *P*-wave velocities, layer thicknesses, densities and estimated resolutions of the final model.

Model layer	<i>P</i> -wave velocity (km s <sup>-1</sup> )			Density (g cm <sup>-3</sup> )	
	Top	Bottom	Thickness (km)	Top	Bottom
Water:	1.49	1.52	Variable	1.03	1.03
Sediments:					
<i>S1</i>	1.62 ± 0.15	2.46 ± 0.15	0.95 ± 0.07	1.62	2.18
<i>S2</i>	2.38 ± 0.15	2.75 ± 0.15	0.50 ± 0.15	2.08	2.27
<i>S3</i>	2.70 ± 0.15	3.06 ± 0.15	0.45 ± 0.20	2.21	2.29
<i>S4</i>	2.85 ± 0.20	3.12 ± 0.20	1.55–2.55 ± 0.20	2.24	2.32
<i>S5</i>	3.20 ± 0.20	4.70 ± 0.20	1.00–2.20 ± 0.30	2.32	2.50
Crust:					
Oceanic					
<i>Layer 2</i>	4.60 ± 0.30	5.70 ± 0.30	1.50–2.00 ± 0.45	2.49	2.81
<i>Layer 3</i>	6.40 ± 0.45	7.50 ± 0.45	2.00–3.00 ± 0.80	2.87	3.01
Continental					
Upper crust	5.60 ± 0.45	6.00 ± 0.45	5.00 ± 0.45	2.54	2.67
Lower crust	6.40 ± 0.15	6.70 ± 0.15	31.00 ± 2.50	2.85	2.95
Mantle:	8.00 ± 0.15	-	-	3.31	-

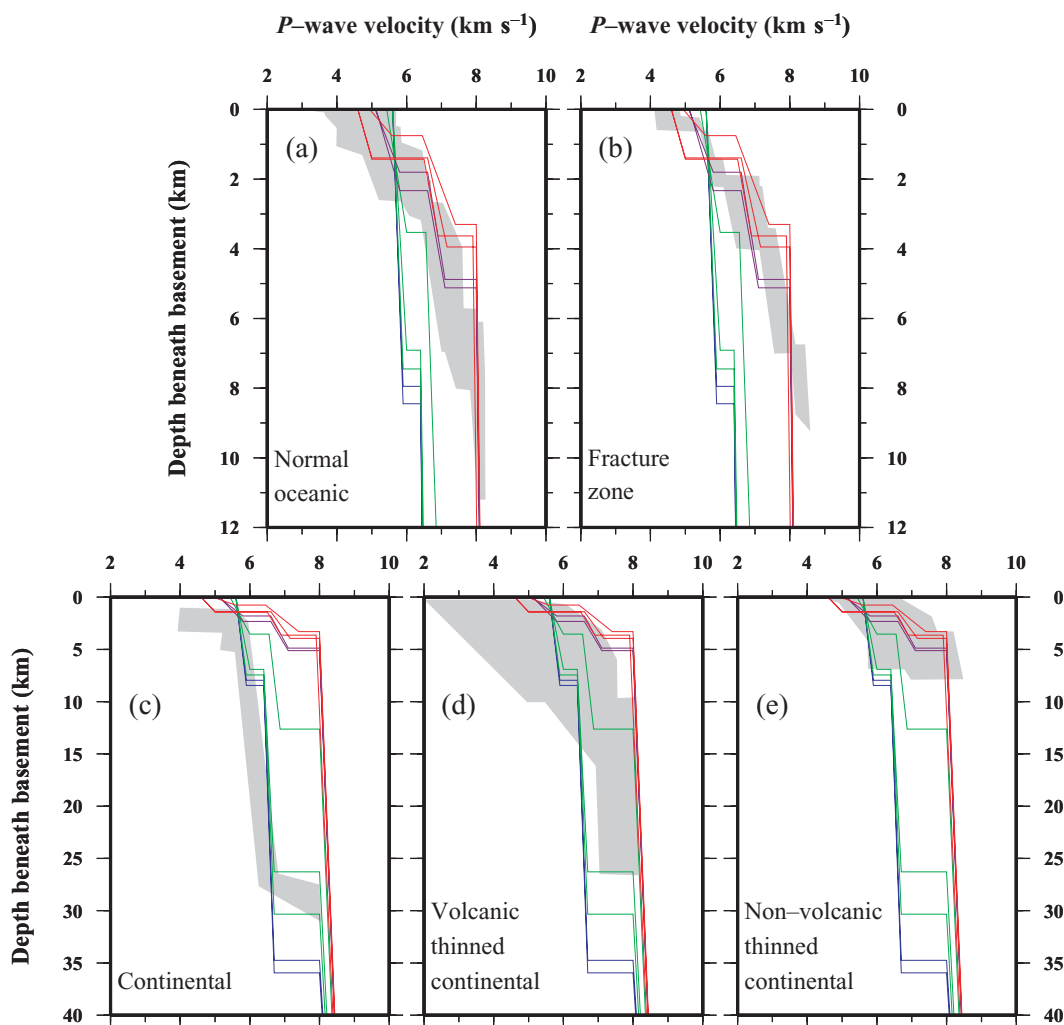


**Figure 14.** Comparison of velocity–depth profiles from the *P*-wave model with compilations for (a) normal oceanic crust, (b) oceanic crust adjacent to fracture zones, (c) continental crust, (d) thinned volcanic continental crust and (e) thinned non-volcanic continental crust. See text for details and references, in addition to Hinz *et al.* (1982), Morgan *et al.* (1989), Morgan (1988), Mutter & Zehnder (1988) and White (1979, 1984) (e.g. Peirce *et al.* 1996). The ACE velocity–depth profiles are colour coded for oceanic crust (red), unthinned continental crust (blue), thinned continental crust (green) and transitional crust (purple). Note how the oceanic crust is significantly thinner than normal.

a maximum sediment cover of 6.4 km, thinning oceanwards to ~4.0 km.

#### 4.3.2 Oceanic crust

The crust seaward of 250 km offset is identified as oceanic from its hummocky basement surface (MCS data) and the distinctive three-layered velocity structure in the WA model (White *et al.* 1992). Immediately beneath the basement surface, oceanic *Layer 2* velocities are poorly constrained as a consequence of few refracted arrivals being recorded. However, *Layer 3* is well constrained, with the highest velocities (7.2–7.5 km s<sup>-1</sup>) found in the lowermost crust between 255 and 340 km offset. The oceanic Moho lies at a depth of ~17 km below sea surface (bss) beneath the edge of the continental shelf shallowing to 10 km beneath the abyssal plain. *Layers 2* and *3* together range in thickness from 3.5–5 km, of which 2–3 km is *Layer 3*.

The high velocities observed at the base of the oceanic crust occupy a region less than 0.7 km thick. These velocities are consistent with those observed within regions interpreted as underplate (Morgan & Barton 1990; Holbrook *et al.* 1994b). However, there is no evidence of SDR sequences within the MCS data to support this interpretation. An alternative interpretation is that the high velocities reflect some degree of serpentinization, possibly as a result of water ingress along large-offset faults or fracture zones within the crust (e.g. Bonatti 1978; Fox & Gallo 1986).

#### 4.3.3 Continental crust

The crust landward of 140 km model offset is identified as continental. Although ray coverage is quite limited in this region due to the acquisition geometry, the WA model shows a two-layered crust, the base of which is constrained at a maximum depth of ~37.5 km by *P<sub>m</sub>P* arrivals, and the Moho shallows slightly seawards to a depth of ~34.5 km at 135 km offset.

#### 4.3.4 Thinned continental crust

The crust between 135 and 206 km model offset is identified as thinned continental in type from its crustal velocity–depth profile which is consistent with global averages from thinned crust imaged in continental margin settings (Fig. 14; Peirce *et al.* 1996). However, the top of the *Upper Crust* layer shows no evidence, either in the WA model or in the MCS data, of the large-scale rotated fault blocks and half graben observed at many rifted continental margins (e.g. Goban Spur—Peddy *et al.* 1989).

By ~206 km model offset the crust has thinned from ~37.5 km to ~5.2 km thick. This thinning is largely accommodated within the upper crust (from 6.5 km to 2.2 km) between 175 and 206 km offset and in lower crust (25.5 km to 3 km) between 135 and 206 km offset. This is equivalent to a shallowing of the Moho from 34.5 to 14.4 km between the continental shelf and the base of the continental rise, and corresponds to thinning by a factor of 6.4 over a distance of 70 km.

#### 4.3.5 Transition zone

The region between 206 and 250 km model offset is identified as a transition zone as it expresses neither distinct oceanic or continental characteristics. It also lies landward of the region of higher velocities identified within the very base of the oceanic crust adjacent to this zone whose location also corresponds to a 1–1.25 km depression in the surface of the basement and thinning of *Layer 2*.

#### 4.3.6 Resolution

Quantitative analysis of the ray-trace traveltimes and the data picks demonstrates that the model fits the data within the error bounds (see Table 1). Although the goal of modelling was to achieve a statistical data fit to within the assigned error bounds on each traveltime pick, using a  $\chi^2$  of <1 as the measure of the misfit for each phase type and each layer separately within the model, not all instruments and phases could be matched within these criteria. For the land instruments, overall all arrivals were modelled to an error of 126 ms and  $\chi^2$  of 1.4. Seaward of OBS 1 the model has a much improved resolution with a total misfit of just 36 ms and a  $\chi^2$  of 0.9.

A fit to within these criteria does not guarantee the uniqueness of the model as traveltimes are dependant upon both seismic velocity and propagation path length. Therefore, an adequate data fit can often be obtained by increasing one and decreasing the other of these parameters and vice versa. However, the resulting model uncertainties associated with this trade-off have been estimated by systematically varying the model parameters and, hence, sensitivity testing modelled horizons and layer velocities. An upper bound on the misfit was also applied above which the model and/or its subparts were considered ‘out of range’. For the OBS/H arrivals a misfit above  $\pm 100$  ms was considered the upper limit (e.g. Edwards *et al.* 1997), while for the land station arrivals this was set at  $\pm 250$  ms. The resulting resolution in velocity and thickness of each model layer is outlined in Table 2.

## 5 GRAVITY MODELLING

Gravity modelling was undertaken primarily as a test of validity and uniqueness of the WA model, and secondly to provide additional constraints on the variation in crustal thickness and Moho geometry beneath the continental slope and shelf where the ray coverage is limited.

The free-air anomaly (FAA) acquired whilst shot firing was used as the basis of the modelling (Fig. 13). This anomaly was also correlated with the satellite-derived anomaly (Sandwell & Smith 1997) to compare the longer-wavelength anomaly characteristics associated with deeper crust and uppermost mantle variation. The FAA is striking in that it is, given the underlying crustal structure, remarkably simple with the most prominent feature being the margin edge effect high (e.g. Watts & Marr 1995). However, the French Guiana margin transect is unusual in that the characteristic accompanying edge effect low on the seaward side of the margin is absent.

### 5.1 Initial model

As a starting point for modelling, the velocity–depth model was initially converted to a density model using the velocity–density relationship of Nafe & Drake (1957) (Ludwig *et al.* 1970), coupled with the relationships of Carlson & Raskin (1984) and Christensen & Mooney (1995). Model densities are quoted in g cm<sup>-3</sup>, mainly for reasons of clarity of annotation on Fig. 13—1 g cm<sup>-3</sup> is equivalent to 1000 kg m<sup>-3</sup> in S.I. units.

The Nafe & Drake (1957) relationship is based on measurements of sediment velocity and density, and thus this method was used primarily to assign initial densities to the *Sediment* layer seaward of the shelf break. Christensen & Mooney’s (1995) velocity–density relationship for the continental crust was used primarily to assign densities landwards of the shelf break, while the relationships of Carlson & Raskin (1984) for the oceanic crust were applied seaward of the shelf break. A density of 1.03 g cm<sup>-3</sup> was assigned to the water

column and the uppermost mantle a density of  $3.31 \text{ g cm}^{-3}$  (Kuo & Forsyth, 1988)—a value commonly used in gravity studies of continental margins (e.g. Wu *et al.* 2006). To best represent the *P*-wave velocity gradients, model layers were also constructed with density gradients following seismic velocity contour geometries with, on average, an increase in velocity of  $0.1 \text{ km s}^{-1}$  correlating with an increase in density of  $0.02 \text{ g cm}^{-3}$ , between  $1.6 \text{ km s}^{-1}$  just below the seabed and  $7.0 \text{ km s}^{-1}$  which defines the base of the crust for the majority of the seismic model.

FAA modelling was carried out using *GRAV2D* (a 2-D approach based on the Talwani *et al.* 1959 algorithm). As the purpose of the 2-D gravity modelling is to test the validity and uniqueness of the seismic modelling, layer boundaries were not varied to improve the gravity fit; the only exception being the depth to Moho between 135 and 200 km, where seismic constraint is limited.

## 5.2 Results

The results of gravity modelling are shown in Fig. 13 and layer densities are summarized in Table 2. Overall, the fit between the calculated and observed anomalies is excellent, lying well within the associated error for the majority of the profile for the preferred model. The most significant misfits are centred on:

- (i) 180 km offset, at the peak of the margin edge effect. This misfit most likely results from the depth and geometry of the Moho in this region of the model, though may also reflect the lack of constraint on sediment thickness on the continental shelf due to an absence of clear MCS reflections.
- (ii) 240–280 km model offset, the region in which the characteristic flanking low associated with the margin edge effect high would be expected (e.g. Watts & Marr 1995). This misfit correlates with the region interpreted as the oceanward limit of the transition zone between thinned continental and oceanic type crust. The nature of the misfit implies either that the crust and/or sediment layers are too thin or that the density is too high.
- (iii) 370–400 km model offset. Towards these longer profile distances the seismic resolution of the sub-sediment crustal layers is limited due to the relative offset between shots and the OBS/Hs at the seaward end of the profile. In addition, the Müller *et al.* (1997) crustal age model (Fig. 15) suggests that a transform/fracture zone intersects Profile A approximately between OBS/Hs 18–20 (Fig. 13) which correlates with a depression in the oceanic crustal basement surface and a thickening of the lowest sediment layer (S5). The gravity misfit implies thinner crust and/or sediment layers or that the model density within this region is too low.

The density-depth model was used to test these possibilities, fixing the Moho depth where the gravity fit was acceptable and varying the model within the 240–280 km and 370–400 km misfit regions. An improved fit can be achieved by an increase in crustal thickness at 260 km offset of around 750 m, and by thinning of the crust at 385 km offset by around 600 m. Despite the dense ray coverage in both these localities, the seismic resolution is not capable of distinguishing between the original model and the adjusted model. However, the gravity modelling also suggests that either a slight increase in Moho depth or a slight decrease in crustal density, perhaps as a result of serpentinization, is the cause of the misfit around 240–280 km offset, and that crustal thinning is the most likely origin of the misfit around 385 km offset.

## 6 DISCUSSION

The ACE aimed to reveal crustal structural variation along the equatorial continental margin of South America and determine the geometry and mode of opening of the Atlantic and the role, if any, played by magmatism during rifting. This margin was chosen for study since it is located proximal to a region of numerous transform faults, which currently offset the MAR (Fig. 2). The corresponding fracture zones appear to be long-lived features associated with, or resulting from, the initial break-up geometry since they can be traced from the MAR to each margin and appear correlated with the along-margin variation between rift-type and transform-type settings (Fig. 15). In this context, Profile A was located across the French Guiana margin within a region thought to be of rift-type.

### 6.1 Volcanic versus non-volcanic margin

Deep crustal seismic studies of the Atlantic margins have shown that continental rifting does not always take place by a process of simple stretching followed by thermal subsidence (Sleep 1971; McKenzie 1978) but may also be associated with massive thicknesses of igneous material (Mutter *et al.* 1984; White *et al.* 1987; Holbrook *et al.* 1994a) accreted into the crust. These observations led to passive margins being classified as either volcanic or non-volcanic (sedimentary) in type. Volcanic margins are characterized by a sequence of lower crustal rocks up to 25 km thick (White *et al.* 1987; White, 1992), with high velocities in the range  $7.2\text{--}7.5 \text{ km s}^{-1}$  in a region that is commonly termed as underplate. Volcanic margins are also characterized by SDR sequences, which are interpreted as subaerial basaltic flows erupted during the early stages of initial rifting. In contrast non-volcanic margins lack these volcanic features and instead exhibit faulted basement blocks, and for the Atlantic in particular, no distinct boundary between thinned continental crustal and normal oceanic crust (Dean *et al.* 2000). As progressively more studies of volcanic and non-volcanic margins are undertaken, results suggest that this characterization may be over-simplistic (Mutter 1993; Holbrook *et al.* 1994a) and that instead the majority of margins express volcanic characteristics to some extent (Eldholm *et al.* 1995; Geoffroy 2005).

Interpretation of the ACE WA model for Profile A shows no evidence of velocities in excess of  $7.0 \text{ km s}^{-1}$  in the lower crust within the regions identified as continental in origin. In addition, interpretation of the coincident MCS data reveals no evidence of SDR sequences, although it has been suggested that such sequences may not always have clear reflection events associated with them (Eldholm & Grue 1994; Planke & Eldholm 1994; Planke *et al.* 2000; Geoffroy 2005). The continental margin offshore French Guiana in the region imaged by Profile A is therefore interpreted as a non-volcanic margin. Consequently, all further discussion and comparisons will be made with reference to other non-volcanic Atlantic rifted margins. However, the role of transform faults and fracture zones in continental break-up geometry, margin evolution and crustal structural development will also be considered by reference to the equatorial west Africa transform margins (Fig. 1).

### 6.2 Rifting versus transform margin evolution

The pre-rift continental crust along Profile A is 34–37 km thick, comparable with other margins of the Atlantic. For example, at the Nova Scotia (Funck *et al.* 2004) and Orphan Basin (Chian *et al.* 2001) rifted margins the pre-rift crustal thickness has been determined at  $\sim 36$  km. Similar estimates of  $\sim 36\text{--}41$  km have been

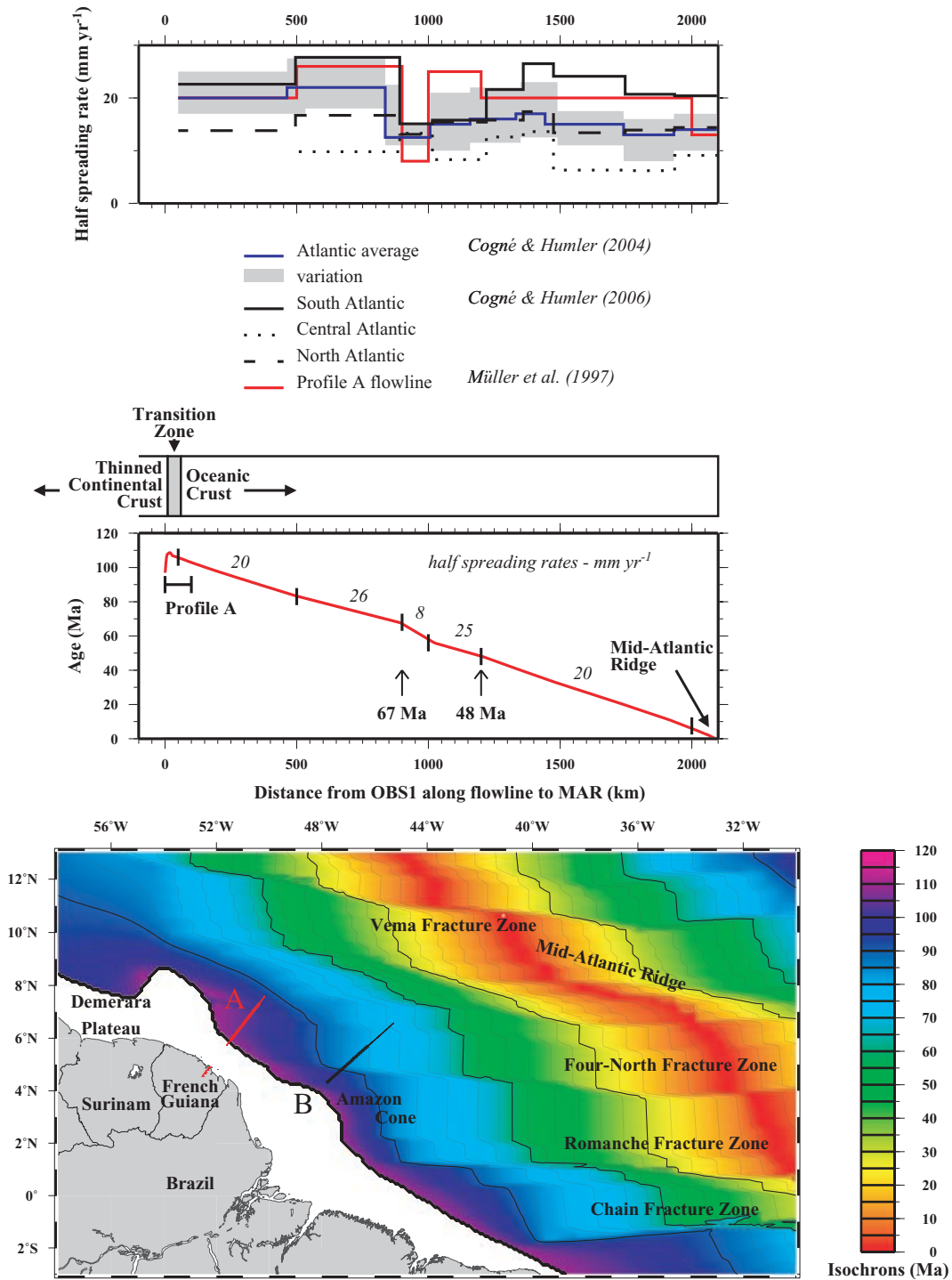


**Figure 15.** Initial seafloor spreading rate at the French Guiana margin. Bottom: Müller *et al.*'s (1997) seafloor age isochrons for the west equatorial Atlantic, showing fracture zone traces and the MAR. ACE Profiles A & B are shown by solid lines (shots: thin lines; OBS/H: thick lines). Isochrons are plotted at 30 Ma intervals. Middle: Half-spreading rate from inception of seafloor spreading to present day along a flow-line from Profile A. Top: Comparison of spreading rate at Profile A with the average values for Cogné & Humler's (2004, 2006) South, Central and North Atlantic regions. The variation in spreading rate between 67 and 48 Myr is thought to be associated with adjustment in opening geometry as a result of the onset of northwards migration of the Indian continent (Fig. 3).

obtained along multiple transects of the US East Coast (e.g. LASE Study Group 1986; Tréhu *et al.*, 1989; Holbrook and Keleman 1993; Sheridan *et al.* 1993; Holbrook *et al.* 1994a,b). Edwards *et al.* (1997) used gravity modelling to estimate the pre-rift continental thickness at 35 km close to the Ghana margin. However, this thickness is not

'standard' as many examples of significantly thinner crust are also observed, such as ~27 km at both the Goban Spur (Horsefield *et al.* 1993) and Iberia (Dean *et al.* 2000) margins.

Another common feature of rifted margins are tilted block and half graben structures, which form large, fault bounded

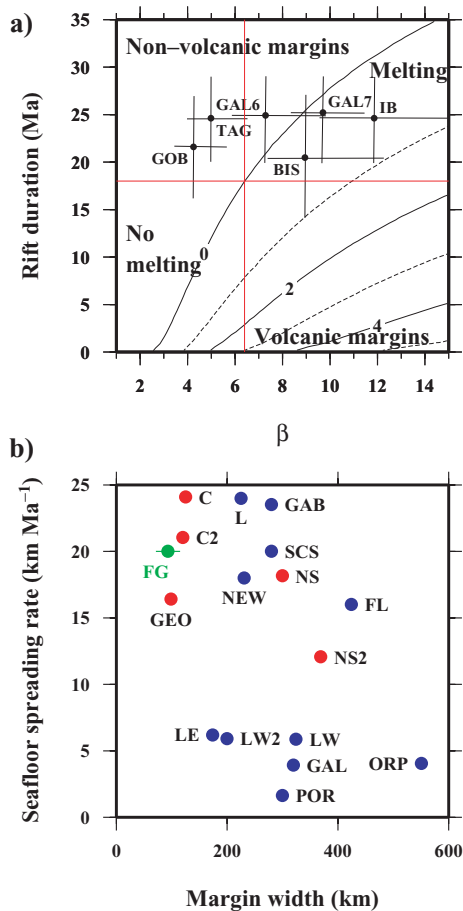


**Figure 16.** Comparison of the French Guiana margin with seafloor spreading rates, rift duration and extension, and margin width observed at other rifted margins. (a) Variation in melt thickness relative to crustal thinning ( $\beta$ ) after Bown & White (1995). (b) Initial half seafloor spreading rate plotted against margin width after Davis & Kuszniir (2002). The French Guiana margin is marked in red (a) and green (b). Example margins: C & C2 = Carolina; L = LASE; SCS = South China Sea; FL = Flemish Cap; ORP = Orphan; POR = Porcupine Basin; GAL, GAL6 & GAL7 = Galicia; LW & LW2 = West Labrador; LE = East Labrador; NS & NS2 = Nova Scotia; NEW = Newfoundland; GEO = St George's Bank; GAB = Gabon; IB = Iberia; BIS = Biscay; and TAG = Tagus Abyssal Plain. See Bown & White (1995) and Davis & Kuszniir (2002) for details and references for these margins contained therein. Assuming a stretching factor of 6.4 derived from the *P*-wave model (Fig. 13) and that there is no evidence from Profile A for rift-related magmatism, Bown & White's (1995) model predicts a minimum rift duration of 18 Myrs. Similarly a margin width of  $\sim 70$  km and an initial spreading half-rate of  $20 \text{ mm yr}^{-1}$  (Fig. 15—after Müller *et al.* 1997), suggests that the French Guiana margin formed, when compared with other margins, relatively rapidly with extension confined to a relatively narrow region.

basins. Examples of such structures are found at the Goban Spur (Horsefield *et al.* 1993), Biscay (Montadert *et al.* 1979, de Charpal *et al.* 1978), Rockall (England & Hobbs 1997) and Iberia (Pickup *et al.* 1996) margins. The French Guiana margin (along Profile A) does not display any rotated faulted block characteristics, instead the WA model shows the pre-rift continental crust comprising, primarily, crystalline basement with a smooth surface, overlain with a thin veneer of sediments. Thus, although showing no evidence of volcanic features, the French Guiana margin appears atypical when compared to other non-volcanic margins.

Along Profile A, the crystalline basement thins by a factor of up to 6.4 ( $\beta$  factor) over  $\sim 70$  km distance and this thinning is accompanied by a transition zone  $\sim 45$  km wide (see Section 6.3), a total combined width of  $\sim 115$  km. The rapidity of thinning and the width of the transition reveal much about the nature of a margin and its mode of evolution, with the distance over which thinning occurs generally being smaller for transform margins than for rifted margins. Dean *et al.* (2000) summarize measurements of the width of regions of thinned continental ( $\sim 80$ – $150$  km) and transition zone (10–120 km) crust and conclude that the typical combined width for the North Atlantic is 100–200 km. At 115 km at most, the French Guiana margin lies at the lower end of that range.

Watts & Fairhead (1997) and Davis & Kuszniir (2002) summarize the degree of thinning at Atlantic margins as a function of distance from the OCT (Fig. 16). Watts & Fairhead (1997) conclude that margins can be classified into two types—narrow ( $< 75$  km) and wide ( $> 250$  km) rifts—depending on the distance landward of the OCT over which extension occurs. Under this terminology the French Guiana margin could be described as a narrow rift. However, Davis & Kuszniir (2002) conclude that such a definition is too simplistic and instead use margin width which they define as the distance from pre-rift, unstretched crust to the ocean–continent boundary (OCB). Davis & Kuszniir (2002) assume the OCB is a sharp transition, rather than the wide transition zone (hence the preferred term OCT) observed at many margins (e.g. Pickup *et al.* 1996), which is commonly interpreted as serpentinized upper mantle exhumed before the onset of seafloor spreading (e.g. Whitmarsh *et al.* 2001).

Despite the uncertainty associated with this assumption, Davis & Kuszniir (2002) show that highly extended margins are associated with slow initial post-break-up seafloor spreading rates and vice versa. Using their model, the initial seafloor spreading rate at the French Guiana margin is anticipated to be relatively high. Müller *et al.*'s (1997) seafloor isochrons for the Atlantic estimate the initial, post-rift half-spreading rate at the French Guiana margin at  $\sim 20 \text{ mm yr}^{-1}$  (Fig. 15), and that the spreading rate has varied over time to the present day. Relative to global mid-ocean ridge spreading rates,  $\sim 20 \text{ mm yr}^{-1}$  half-rate is at the upper end of the *slow* category (Dick *et al.* 2003). This spreading rate and the margin width of  $\sim 70$ – $115$  km implies that the French Guianan margin was subject to relatively high strain rates during rifting.

Bown & White's (1995) relationship (Fig. 16) between melt thickness and crustal thinning ( $\beta$ ) shows that (assuming the initial thickness of the lithosphere and temperature of the underlying mantle remain constant) the longer the rift duration, the less melt is produced (Contrucci *et al.* 2004). A  $\beta$  factor of 6.4, and assuming that the French Guiana margin is non-volcanic, provides an estimate of rift duration of at least 20 Myr. This is consistent with the proximal non-volcanic Angola margin where the duration of rifting has been estimated between 15 and 30 Myr (Moulin 2003).

The variation in half-spreading rate along a flow-line from OBS 1 to the MAR, suggests that the west equatorial region is most similar to Cogné & Humler's (2004, 2006) compilations for their South Atlantic region ( $0^\circ$ – $55^\circ$ S) except between 67 and 48 Ma (chrons 31–21) which corresponds to the rapid northwards migration of the Indian plate (Cogné & Humler 2004), the reorientation of spreading in the South Atlantic in response to the rotation of South American plate relative to North American plate and the onset of transform-style separation between equatorial West Africa and Northeast Brazil (Patriat & Achache 1984; Besse & Courtillot 2002). An alternative interpretation for the narrow margin width is, thus, that instead the French Guiana margin is a transform margin.

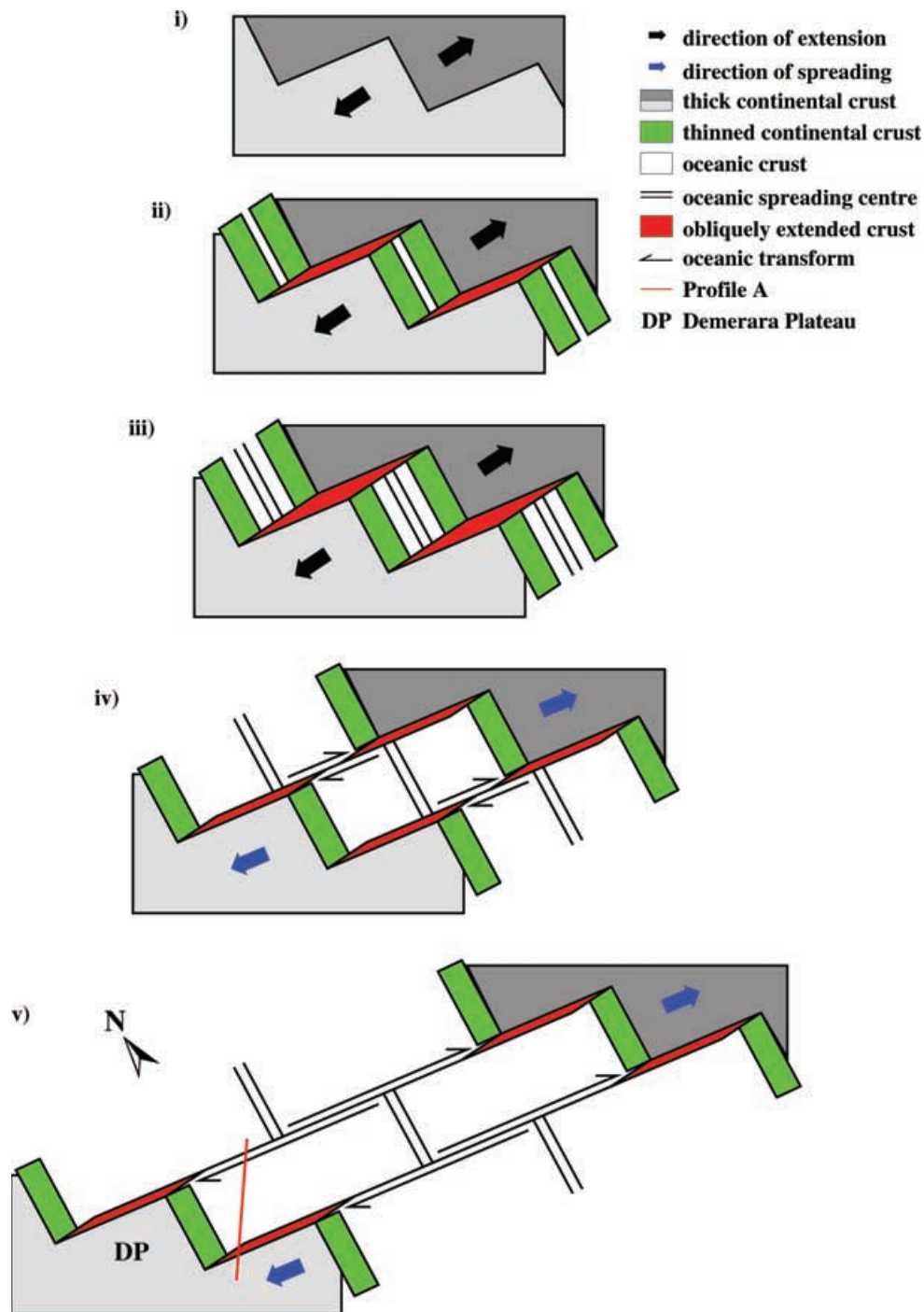


**Figure 17.** Simplified model of margin evolution (after Peirce *et al.* 1996, and developed from Mascle & Blarez 1987 and Mascle *et al.* 1997). (i) Initial intracontinental transform rifting of the African and South American plates. (ii) Thinned continental crust in rift segments separated by transforms. (iii-iv) Oceanic spreading resulting in the juxtaposition of old continental lithosphere against young oceanic lithosphere. (v) Juxtaposition of thinned continental crust against normal thickness oceanic crust across a fracture zone, showing the current setting of Profile A (red) explaining the narrow margin width, degree of thinning and the lack of observed rift-related extensional structures in the upper basement.

In general, transform margins (e.g. Scrutton 1979; Newfoundland—Todd *et al.* 1988; Barents Sea—Jackson *et al.* 1990; Exmouth Plateau—Lorenzo *et al.* 1991) are characterized by a zone of apparent crustal thinning 5–30 km wide, an absence of the high lower crustal velocities indicative of magmatism and an absence of basement rotated fault blocks. Although the French Guiana margin shares many characteristic features with

non-volcanic margins, its narrow margin width and lack of rotated fault blocks suggest that the break-up geometry in this part of the equatorial Atlantic has a significant transform component.

Regions of underplate are observed at transform margins (e.g. Southern Exmouth Plateau margin—Lorenzo *et al.* 1991). At the Ivory Coast-Ghana transform margin Peirce *et al.* (1996) observe underplate which they interpret as a localized feature since other

parts of the adjacent Ghana margin show no such evidence (e.g. Edwards *et al.* 1997). Peirce *et al.* (1996) attribute this lateral variation to a mode of margin evolution in which dominant transform motion is accompanied by a component of rifting (Fig. 17), and which results in a margin composed of a series of rift and transform segments (Masclé *et al.* 1997).

Wilson *et al.* (2003) describe the architecture of the equatorial West Africa margin (Gabon, Guinea and Cameroon). At this transform margin, the transition from oceanic to continental crust occurs over 75 km, with the crust neither being typically oceanic or continental within this region. Wilson *et al.* (2003) interpret this crust as serpentinized peridotite and attribute it to the existence of numerous fracture zones which allow the ingress of sea water and serpentinization by hydrothermal circulation, of which one mechanism is via fracturing associated with trans-tension or oblique-slip motion.

### 6.3 Oceanic crustal thickness

Oceanic crustal thickness is, on average,  $7.1 \pm 0.8$  km, of which  $2.11 \pm 0.55$  km is oceanic extrusive *Layer 2* and  $4.97 \pm 0.90$  km is intrusive *Layer 3* (Fig. 14; White *et al.* 1992). However, oceanic crustal thickness along Profile A is only 3.5–5.0 km. When compared with local and conjugate margins this thinness is less surprising. For example, the average thickness of oceanic crust offshore Ghana is 4.4 km (Edwards *et al.* 1997), offshore Gabon-Guinea-Cameroon 5 km (Wilson *et al.* 2003) and Congo-Zaire-Angola 5–8 km (Watts & Stewart 1998; Contrucci *et al.* 2004).

Thin oceanic crust is found in three main settings (Edwards *et al.* 1997); at mid-ocean ridges spreading at ultra-slow rates ( $<15$  mm yr<sup>-1</sup> full rate—Bown & White 1995) where conductive cooling of the upwelling mantle results in a reduction in the amount of melt produced; adjacent to non-volcanic rifted margins (bordering the Atlantic—Whitmarsh *et al.* 1990, 1993; Pinheiro *et al.* 1991; Horsefield *et al.* 1993) where conductive heat loss in the mantle results from long-lasting stretching of the continental lithosphere prior to break-up (Whitmarsh *et al.* 1993; Bown & White 1995); and at oceanic transform faults/fracture zones, which White *et al.* (1984, 1992) and Minshull *et al.* (1991) attribute to a reduced magma supply to the adjacent mid-ocean ridge segment tips, and Stroup & Fox (1981) and Fox & Gallo (1984) attribute to an enhanced cooling effect of adjacent colder lithosphere when offsets are large.

In this study we estimate that the initial full spreading rate at the French Guiana margin is  $\sim 40$  mm yr<sup>-1</sup>. Thus it is unlikely that the thin oceanic crust is a result of initial ultra-slow spreading. The extent of crustal thinning ( $\beta$  factor of 6.4) which has occurred within the relatively narrow margin width ( $\sim 70$  km) and the lack of evidence of rift-related magmatism, implies a rift duration of at least 18 Myr (Bown & White 1995). The observed thin oceanic crust may simply be the result of a mantle cooled during a prolonged period of continental rifting prior to the inception of seafloor spreading.

However, another possibility is that the oceanic crustal production rate was lower during the early Cretaceous than at present. Cogné & Humler (2004, 2006) consider this possibility and use compositional changes to assess mantle temperature variation from the present to 180 Ma which, in turn, they use to quantify the volume of magma generated in a spreading ridge setting. Cogné & Humler (2006) conclude that crustal thicknesses were, on global average,  $\sim 1$ –2 km thicker than present before 80 Ma. Thus, it seems unlikely that the relatively thin oceanic crust is due to a low melt production rate per

se, for example, due to a slow-spreading rate and/or a low mantle temperature, but instead has another cause.

Figs 2 and 15 show that the MAR in the equatorial Atlantic between 6°N and 12°N is divided into numerous, relatively short (in Atlantic terms) ridge segments offset by transform faults/fracture zones and shorter non-transform ridge discontinuities (Macdonald 1982) whose orientation and existence can be traced back to the time of continental break-up. Such closely spaced ridge offsets and their associated ridge tip reduced magma budgets, may also give the appearance of anomalously thin crust.

## 7 CONCLUSIONS

The geophysical data collected over the continental margin of French Guiana, as part of the Amazon Cone Experiment, provide a new insight into the deep structure of the crust offshore northeast South America. Forward modelling of WA seismic data collected by 20 ocean-bottom and five land-based instruments, has resulted in a *P*-wave velocity–depth model that shows the structure of pre- and post-rift crust and the nature and extent of the ocean–continent transition, and which is consistent with both the coincident MCS and gravity data.

The margin is characterized by: pre-rift continental crust 34–37 km thick, with seismic velocities ranging from 5.6–6.7 km s<sup>-1</sup>; thinned continental crust in a zone  $\sim 70$  km in width landward of the continental rise-slope transition, and in which the crust thins by a factor of 6.4; an  $\sim 45$ -km-wide ocean–continent transition; oceanic crust, comprising two distinct layers of velocities 4.6–5.7 km s<sup>-1</sup> and 6.4–7.5 km s<sup>-1</sup> and a thickness of 3.5–5.0 km; and, finally, a sediment column up to 6.4 km thick and comprising five layers consistent with the margin-wide pattern of syn- and post-rift deposition.

The  $\sim 70$ -km-wide zone of continental thinning distinguishes this margin from pure transform margins, which commonly show thinning over 10–40 km. However, the French Guiana margin may not be characterized as an obviously normal rifted margin since there is no evidence of rotated faulted block, half-graben structures. In turn, there is no evidence for significant rift-related magmatism, either as SDR sequences or as a high-velocity region within the lower crust. Therefore, the French Guiana margin is most likely a non-volcanic margin which has experienced a component of transform/trans-tensional motion as part of continental break-up.

We therefore conclude that the French Guiana margin displays characteristics indicative of both rifted and transform margins and its features are consistent with the rift-transform models of Masclé *et al.* (1997) and Masclé & Blarez (1987) as applied to the Ivory Coast-Ghana margin in Peirce *et al.* (1996). Fig. 17 shows a version of this model developed to fit the Profile A results. This model accounts for both rift and transform features, a wider margin width than average for transform margins and also the anomalously thin oceanic crust observed.

## ACKNOWLEDGMENTS

We wish to thank the master, officers and crew of the *RRS Discovery*, together with the sea-going staff of NERC's UKORS, Tom Oliva of Seamap UK, and Anne Krabbenhöft and Cord Papenburg who operated the IFM-Geomar seabed instruments during the cruise. Land-based assistance was provided by Dr Jesus Berrocal, Prof Cleverson Silva, and Prof Alberto Figueiredo in Brazil, Andy Louch in NERC's RSU, Lourenildo Leite in Belem and Phillippe Weng and Pierre Laporte in French Guiana. This research was funded by the

UK's NERC through the Ocean Margins LINK programme. RWH was supported by the NERC as an Advanced Research Fellow. The GMT and Seismic Unix software packages (Wessel & Smith (1998) and Cohen & Stockwell (2000) respectively) were used to create the figures for this paper. We thank the two anonymous reviewers for their comments, which greatly improved the clarity of this paper.

## REFERENCES

- Bauer, K. *et al.*, 2000. Deep structure of the Namibia continental margin as derived from integrated geophysical studies, *J. geophys. Res.*, **105**(B11), 25829–25853.
- Benjamin, M., Johnson, N. & Naeser, C., 1987. Recent rapid uplift in the Bolivian Andes—evidence from fission-track dating, *Geology*, **15**(7), 680–683.
- Benkheilil, J., Mascle, J. & Tricart, P., 1995. The Guinea continental margin: an example of a structurally complex transform margin, *Tectonophysics*, **248**, 117–137.
- Besse, J. & Courtillot, V., 2002. Apparent and true polar wander and the geometry of the geomagnetic field over the last 200 Myr, *J. geophys. Res.*, **107**(B11), 2300; doi:10.1029/2000JB000050.
- Blarez, E., 1986. La marge continentale de Côte d'Ivoire-Ghana. Structure et évolution d'une marge continentale transformante. *Ph.D. thesis*, 188 pp., Univ Pierre et Marie Curie, Paris.
- Bonatti, E., 1978. Vertical tectonism in oceanic fracture zones, *Earth Planet Sci. Letts.*, **37**, 369–379.
- Bown, J.W. & White, R.S., 1995. Effect of finite extension rate on melt generation at rifted continental margins, *J. geophys. Res.*, **100**(B9), 18011–18029.
- Braga, L.F.S. 1991. Isostatic evolution and crustal structure of the Amazon continental margin determined by admittance analysis and inversion of gravity data. *Ph.D. Thesis* (unpublished), Oregon State University, Corvallis.
- Brandão, J.A.S.L. & Feijó, F.J., 1994. Bacia do Foz do Amazonas, *Boletim de Geociências da Petrobrás (Rio de Janeiro)*, **8**(1), 91–100.
- Bratt, S.R. & Purdy, G.M., 1984. Structure and Variability of Oceanic Lithosphere on the Flanks of the East Pacific Rise Between 11° and 13°, *J. geophys. Res.*, **89**, 6111–6125.
- Bullock, A.D. & Minshull, T.A., 2005. From continental extension to seafloor spreading: crustal structure of the Goban Spur rifted margin, southwest of the UK, *Geophys. J. Int.*, **163**, 527–546.
- Callot, J.-P. & Geoffroy, L., 2002. Development of volcanic passive margins: three-dimensional laboratory models, *Tectonics*, **21**, doi:10.1029/2001TC901019.
- Carlson, R.L. & Raskin, G.S., 1984. Density of the ocean crust, *Nature*, **311**, 555–558.
- Castro, J.C., Miura, K. & Braga, J.A.E., 1978. Stratigraphic and structural framework for the Foz do Amazonas basin. *Society of Petroleum Engineers 10th Annual Offshore Technology Conf. Proc.*, **3**, 1843–1847.
- Chian, D., Reid, I.D. & Jackson, H.R., 2001. Crustal structure beneath Orphan Basin and implications for nonvolcanic continental rifting, *J. geophys. Res.*, **106**, 10923–10940.
- Christensen, N.I. & Mooney, W.D., 1995. Seismic velocity structure and composition of the continental crust: a global view, *J. geophys. Res.*, **100**(B6), 9761–9788.
- Cobbold, P.R., Mourges, R. & Boyd, K., 2004. Mechanism of thin-skinned detachment in the Amazon Fan: assessing the importance of fluid overpressure and hydrocarbon generation, *Marine Pet. Geology*, **21**, 1013–1025.
- Cogné, J.-P. & Humler, E., 2004. Temporal variation of oceanic spreading and crustal production rates during the last 180 My, *Earth Planet Sci. Letts.*, **227**, 427–439.
- Cogné, J.-P. & Humler, E., 2006. Trends and rhythms in global seafloor generation rate, *Geochem. Geophys. Geosyst.*, **7**, Q03011, doi:10.1029/2005GC001148.
- Cohen, J. & Stockwell, J., 2000. CWP/SU: Seismic Unix release 34: a free package for seismic research and processing, *Centre for Wave Phenomenon, Colorado School of Mines*.
- Contrucci, I. *et al.*, 2004. Deep structure of the West African continental margin (Congo, Zaïre, Angola), between 5°S and 8°S, from reflection/refraction seismics and gravity data, *Geophys. J. Int.*, **158**, 529–553.
- Damuth, J.E. & Kumar, N., 1975. Amazon Cone: morphology, sediments, age and growth pattern, *Geol. Soc. Am. Bull.*, **86**, 863–878.
- Davis, M. & Kusznir, N., 2002. Are buoyancy forces important during the formation of rifted margins? *Geophys. J. Int.*, **149**, 524–533.
- de Charpal, O., Guennoc, P., Montadert, L. & Roberts, D.G., 1978. Rifting, crustal attenuation and subsidence in the Bay of Biscay, *Nature*, **275**, 706–711.
- Dean, S.M., Minshull, T.A., Whitmarsh, R.B. & Loudon, K.E., 2000. Deep structure of the ocean-continent transition in the southern Iberia Abyssal Plain from seismic refraction profiles: the IAM-9 transect at 40° 20'N, *J. Geophys. Res.*, **105**(B3), 5859–5885.
- Dick, J.J.B., Lin, J. & Schouten, H., 2003. An ultraslow-spreading class of ocean ridge, *Nature*, **426**, 405–411.
- Edgar, T. & Ewing, J., 1968. Seismic refraction measurements on the continental margin of northeastern South America, *Am. Geophys. Union Trans.*, **49**, 197–198.
- Edwards, R.A., Whitmarsh, R.B. & Scrutton, R.A., 1997. The crustal structure across the transform continental margin off Ghana, eastern equatorial Atlantic, *J. Geophys. Res.*, **102**(B1), 747–772.
- Eldholm, O. & Grue, K., 1994. North Atlantic volcanic margins: dimensions and production rates, *J. geophys. Res.*, **99**, 2955–2968.
- Eldholm, O., Skegseid, J., Planke, S. & Gladchenko, T.P., 1995. Volcanic margins concepts. In: Banda, E., *et al.* (eds), *Rifted Ocean-Continent Boundaries*, NATO ASI Ser., **963**, 1–16, Springer, New York.
- England, R.W. & Hobbs, R.W., 1997. The structure of the Rockall Trough imaged by deep seismic reflection profiling, *J. Geol. Soc. Lond.*, **154**, 497–502.
- Erbacher, J., Mosher, D.C., Malone, M.J. *et al.*, 2004. *Proc. ODP Init. Repts.*, 207, College Station, TX (Ocean Drilling Program); doi:10.2973/odp.proc.ir.207.2004.
- Fox, P.J. & Gallo, D.G., 1984. A tectonic model for ridge-transform-ridge plate boundaries: implications for the structure of oceanic lithosphere, *Tectonophysics*, **104**, 205–242.
- Fox, P.J. & Gallo, D.G., 1986. The geology of North Atlantic transform plate boundaries and their aseismic extensions. In: Vogt, P.R. & Tucholke, B.E. (eds), *The Geology of North America*, vol. M, *The Western North Atlantic Region*, *Geol. Soc. America*, 157–172.
- Funck, T., Jackson, H.R., Loudon, K.E., Dehler, S.A. & Wu, Y., 2004. Crustal structure of the northern Nova Scotia rifted continental margin (eastern Canada), *J. Geophys. Res.*, **109**, B09102; doi:10.1029/2004JB003008.
- Geoffroy, L., 2005. Volcanic passive margins, *C.R. Geosci.*, **337**, 1395–1408.
- Gouyet, S., Unternehr, P. & Mascle, A., 1993. The French Guyana margin and the Demerara Plateau: geological history and petroleum plays. In: A. Mascle (ed), *Hydrocarbon and petroleum geology of France*, pp. 411–422.
- Hinz, K., Dostmann, H. & Fitsch, J., 1982. The continental margin of Morocco: seismic sequences, structural elements and geological development. In: Von Rad, U., Hinz, K., Santhein, M. and Seibold, E. (eds), *Geology of the Northwest Africa Continental Margin*, Springer-Verlag, New York, pp. 34–60.
- Holbrook, W.S. & Keleman, P.B., 1993. Large igneous province on the US Atlantic margin and implications for magmatism during continental breakup, *Nature*, **364**, 433–436.
- Holbrook, W.S., Purdy, G.M., Sheridan, R.E., Gover, L., III, Talwani, M., Ewing, J. & Hutchinson, D., 1994a. Seismic structure of the U.S. Mid-Atlantic continental margin, *J. geophys. Res.*, **99**, 17871–17891.
- Holbrook, W.S., Reiter, E.C., Purdy, G.M., Sawyer, D., Stoffa, P.L., Austin Jr., J.A., Oh, J. & Makris, J., 1994b. Deep structure of the U.S. Atlantic continental margin, offshore South Carolina, from coincident ocean bottom and multichannel seismic data, *J. geophys. Res.*, **99**, 9155–9178.
- Horsefield, S.J., Whitmarsh, R.B., White, R.S. & Sibuet, J.-C., 1993. Crustal structure of the Goban Spur rifted continental margin, NE Atlantic, *Geophys. J. Int.*, **119**, 1–19.
- Houtz, R.E., 1977. Sound-velocity characteristics of sediment from the eastern South American margin, *Geol. Soc. Am. Bull.*, **88**, 720–722.

- Houtz, R.E., Ludwig, W.J., Milliman, J.D. & Grow, J.A., 1977. Structure of the northern Brazil continental margin, *Geol. Soc. Am. Bull.*, **88**, 711–719.
- Jackson, H.R., Faleide, J.I. & Eldholm, O., 1990. Crustal structure of the sheared Southwestern Barents Sea continental margin, *Mar. Geol.*, **93**, 119–146.
- Kuo, B.Y. & Forsyth, D.W., 1988. Gravity anomalies of the ridge-transform system in the south Atlantic between 31° and 34.5°S upwelling centres and variations in crustal thickness, *Mar. Geophys. Res.*, **10**, 205–232.
- LASE Study Group, 1986. Deep structure of the US East Coast passive margin from large aperture seismic experiments (LASE), *Mar. Pet. Geol.*, **3**, 234–242.
- Lorenzo, J.M., Mutter, J.C., Larson, R.L. & the Northwest Australia Study Group, 1991. Development of the continent-ocean transform boundary of the southern Exmouth Plateau, *Geology*, **19**, 843–846.
- Ludwig, J. W., Nafe, J. E. & Drake, C. L., 1970. Seismic refraction. In: Maxwell, A. E. (ed), *The Sea, Wiley-Interscience*, pp. 53–84.
- Macdonald, K.C., 1982. Mid-ocean ridges: fine scale tectonics, volcanic and hydrothermal processes within the plate boundary zone, *Ann. Rev. Earth Planet Sci.*, **10**, 155–190.
- Masclé, J., 1976. Atlantic-type continental margins: distinction of two basic structural types, *An. Acad. Bras. Cienc.*, **48**, 191–197.
- Masclé, J. & Blarez, E., 1987. Evidence for transform margin evolution from the Ivory Coast-Ghana continental margin, *Nature*, **326**, 378–381.
- Masclé, J., Lohmann, P. & Clift, P., ODP 159 Scientific Party, 1997. Development of a passive transform margin: Côte d'Ivoire-Ghana Transform margin—ODP 159 preliminary results, *Geomarine Letters*, **17**(1), 4–11.
- McKenzie, D.P., 1978. Some remarks on the development of sedimentary basins, *Earth Planet. Sci. Letts.*, **40**, 23–32.
- Mello, M.R. et al., Mosmann, R., Silva, S.R.P., Maciel, R.R. & Miranda, F.P., 2001. Foz do Amazonas area: the last frontier for elephant hydrocarbon accumulations in the South Atlantic realm. In: M.W. Downey, J.C., Threet, and W.A. Morgan (ed), *Petroleum provinces of the twenty-first century: AAPG Memoir*, **74**, pp. 403–414.
- Minshull, T.A., Dean, S.M., White, R.S. & Whitmarsh, R.B., 2001. Anomalous melt production after continental break-up in the southern Iberia Abyssal Plain. In: Wilson, R.C.L., Whitmarsh, R.B., Taylor, B. & Froitzheim, N. (eds), *Non-volcanic rifting of continental margins: a comparison of evidence from land and sea*, Geological Society, London, London, pp. 537–550.
- Mjelde, R., Raum, T., Myhren, B., Shimamura, H., Murai, Y., Takanami, T., Karpuz, R. & Naess, U., 2005. Continent-ocean transition on the Vøring Plateau, NE Atlantic, derived from densely sampled ocean bottom seismometer data, *J. Geophys. Res.*, **110**, B05101; doi:10.1029/2004JB003026.
- Montadert, L., Roberts, D.G., DeCharpal, D., Guennic, P. & Sibuet, J.-C., 1979. Rifting and subsidence of the northern continental margin of the Bay of Biscay, *Init. Repts. DSDP*, **48**, 1025–1060.
- Morgan, J.V., 1988. *Seismic studies over Continental Margins*. Ph.D. dissertation, University of Cambridge, Cambridge, 128 pp.
- Morgan, J.V. & Barton, P.J., 1990. A geophysical study of the Hatton Bank volcanic margin: a summary of the results from a combined seismic, gravity and magnetic experiment, *Tectonophysics*, **173**, 517–526.
- Morgan, J.V., Barton, P.J. & White, R.S., 1989. The Hatton Bank continental margin, III. Structure from wide-angle OBS and multichannel seismic refraction profiles, *Geophys. J. Int.*, **98**, 367–384.
- Moulin, M., 2003. Etude géologique et géophysique des marges continentales passives: exemple du Zaïre et de l'Angola. Ph.D Thesis, Univ. Bretagne Occidentale, 142 pp.
- Müller, R.D., Roest, W.R., Royer, J.-Y., Gahagan, L.M. & Sclater, J.G., 1997. Digital isochrons of the world's ocean floor, *J. Geophys. Res.*, **102**(B2), 3211–3214.
- Mutter, J.C., 1993. Margins declassified, *Nature*, **364**, 393–394.
- Mutter, J.C. & Zehnder, C.M., 1988. Deep Crustal Structure and Magmatic Processes: the inception of Seafloor Spreading in the Norwegian-Greenland Sea, in Morton, A.C. & Parson, L.M., Eds. *Early Tertiary Volcanism and the Opening of the NE Atlantic*, Geological Society Special Publication, **39** pp. 35–48.
- Mutter, J.C., Talwani, M. & Stoffa, P.L., 1984. Evidence for a thick oceanic crust adjacent to the Norwegian margin, *J. Geophys. Res.*, **89**, 483–502.
- Nafe, J.E. & Drake, C.L., 1957. Variation with depth in shallow and deep water marine sediments of porosity, density and the velocities of compressional and shear waves, *Geophysics*, **3**, 523–552.
- Nürnberg, D. & Müller, R.D., 1991. The tectonic evolution of the South Atlantic from Late Jurassic to present, *Tectonophysics*, **191**, 27–53.
- Patriat, P. & Achache, J., 1984. India-Eurasia collision chronology has implications for crustal shortening and driving mechanism of plates, *Nature*, **311**, 615–621.
- Peddy, C., Pinet, B., Masson, D.G., Scrutton, R., Sibuet, J.-C., Warner, M.R., Lefort, J.P. & Schroeder, I.J., 1989. Crustal structure of the Goban Spur continental margin, northeast Atlantic, from deep seismic reflection profiling, *J. Geol. Soc.*, **146**, 427–437.
- Peirce, C., Whitmarsh, R.B., Scrutton, R.A., Pontoise, B., Sage, F. & Mascle, J., 1996. Côte d'Ivoire-Ghana margin: seismic imaging of passive rifted crust adjacent to a transform continental margin, *Geophys. J. Int.*, **125**, 781–795.
- Pereira da Siva, S.R., 1989. Bacias da Foz do Amazonas e Para (Aguas Profundas): Une análise sismoestratigráfica, tectosedimentar e termica, *Proc. Conf. Braz. Geol. Soc.*, **2**, 843–852.
- Pickup, S.L., Wilson, R.C.L., Pena dos Reis, R., Whitmarsh, R.B. & Ribeiro, A., 1996. The western Iberia margin: a geophysical and geological overview, *Proc. Ocean Drill. Program Sci. Results*, **149**, 3–23.
- Pinheiro, L.M., Whitmarsh, R.B. & Miles, P.R., 1991. The ocean-continent boundary off the western continental margin of Iberia, II, Crustal structure in the Tagus Abyssal Plain, *Geophys. J. Int.*, **109**, 106–124.
- Planke, S. & Eldholm, O., 1994. Seismic response and construction of seaward dipping wedges of flood basalts, *J. geophys. Res.*, **99**, 9263–9278.
- Planke, S., Symonds, P.A., Alvestad, E. & Skogseid, J., 2000. Seismic volcanostratigraphy of large-volume basaltic extrusive complexes on rifted margins, *J. geophys. Res.*, **105**(B8), 19335–19351.
- Rodger, M., Watts, A.B., Greenroyd, C.J., Peirce, C. & Hobbs, R.W., 2006. Evidence for unusually thin oceanic crust and strong mantle beneath the Amazon Fan, *Geology*, **34**, 1081–1084; doi:10.1130/G22966A.22961.
- Sandwell, D.T. & Smith, W.H.F., 1997. Marine gravity anomaly from Geosat and ERS 1 satellite altimetry, *J. Geophys. Res.*, **102**(B5), 10039–10054.
- Scrutton, R.A., 1979. On sheared passive continental margins, *Tectonophysics*, **59**, 293–305.
- Sheridan, R.E. et al., 1993. Deep seismic reflection data of EDGE U.S. Mid-Atlantic continental margin experiment: implications for Appalachian sutures and Mesozoic rifting and magmatic underplating, *Geology*, **21**, 563–567.
- Silva, S.R.P., Maciel, R.R. & Severino, M.C.G., 1999. Cenozoic tectonics of Amazon Mouth Basin, *Geo-Mar. Letts.*, **18**, 256–262.
- Sleep, N.H., 1971. Thermal effects of the formation of Atlantic continental margins by continental break-up, *Geophys. J. Roy. Astr. Soc.*, **24**, 325–350.
- Spudich, P. & Orcutt, J., 1980. A new look at the seismic velocity structure of the oceanic crust, *Rev. Geophys.*, **18**, 627–645.
- Stewart, J., Watts, A.B. & Bagguley, J., 2000. Three-dimensional subsidence analysis and gravity modelling of the continental margin offshore Namibia, *Geophys. J. Int.*, **141**, 724–746.
- Stroup, J.B. & Fox, P.J., 1981. Geologic investigations in the Cayman Trough: Evidence for thin oceanic crust along the Mid-Cayman rise, *J. Geol.*, **89**, 395–420.
- Supko, P.R., Perch-Nielson, K. et al., 1977. Initial Reports of the Deep Sea Drilling Project, 39, Washington (U.S. Govt. Printing Office), 1139 pp.
- Talwani, M., Worzel, J.L. & Landisman, M., 1959. Rapid gravity computations for two-dimensional bodies with application to the Mendocino submarine fracture zone, *J. Geophys. Res.*, **64**, 49–59.
- Todd, B.J., Reid, I. & Keen, C., 1988. Crustal structure across the southwest Newfoundland transform margin, *Can. J. Earth Sci.*, **25**, 744–759.
- Tréhu, A. M., Ballard, A., Dorman, L.M., Gettrust, J.F., Kligord, K.D. & Schreiner, A., 1989. Structure of the lower crust beneath the Carolina Trough, U.S. Atlantic continental margin, *J. Geophys. Res.*, **94**, 10585–10600.

- Turner, J.P., Rosendahl, B.R. & Wilson, P.G., 2003. Structure and evolution of an obliquely sheared continental margin: Rio Muni, West Africa, *Tectonophysics*, **374**, 41–55.
- Watts, A.B. & Marr, C., 1995. Gravity anomalies and the thermal and mechanical structure of rifted continental margins. In: Banda, E. et al., (eds), *Rifted ocean-continent boundaries*, Kluwer, Dordrecht, pp. 65–94.
- Watts, A.B. & Fairhead, J.D., 1997. Gravity anomalies and magmatism along the western continental margin of the British Isles, *J. Geol. Soc. London*, **154**, 523–529.
- Watts, A.B. & Peirce, C., 2004. Amazon Cone seismic experiment—ACE. RRS Discovery cruise report, Unpublished, pp. 56.
- Watts, A.B. & Stewart, J., 1998. Gravity anomalies and segmentation of the continental margin offshore West Africa, *Earth Planet Sci. Letts.*, **156**, 239–252.
- Wessel, P. & Smith, W.H.F., 1998. New improved version of the Generic Mapping Tools released, *EOS Trans. AGU*, **79**, 579.
- White, R.S., 1979. Oceanic upper crustal structure from variable angle seismic reflection-refraction profiles, *Geophys. J. Roy. Astr. Soc.*, **57**, 683–726.
- White, R.S., 1984. Atlantic Ocean crust: seismic structure of a slow spreading ridge. In: Gass, I.G., Lippard, S.J. & Shelton, A. N. (eds), *Ophiolites and Oceanic Lithosphere*, *Spec. Publ. Geol. Soc. Lond.*, **13**, 34–44.
- White, R.S., 1992. Crustal structure of North Atlantic continental margins, *J. Geol. Soc. Lond.*, **149**, 841–854.
- White, R.S. & McKenzie, D.P., 1989. Magmatism at rift zones: the generation of volcanic continental margins and flood basalts, *J. geophys. Res.*, **94**, 7685–7729.
- White, R.S., Detrick, R.S., Sinha, M.C. & Cormier, M.H., 1984. Anomalous seismic crustal structure of oceanic fracture zones, *Geophys. J.R. Astron. Soc.*, **79**, 779–798.
- White, R.S. et al., 1987. Hatton Bank (northwest UK) continental margin structure, *Geophys. J.R. Astr. Soc.*, **89**, 265–272.
- White, R.S., McKenzie, D. & O’Nions, R.K., 1992. Oceanic crustal thickness from seismic measurements and rare earth element inversions, *J. Geophys. Res.*, **97**(B13), 19683–19715.
- Whitmarsh, R.B., Miles, P.R. & Mauffret, A., 1990. The ocean-continent boundary off the western continental margin of Iberia I. Crustal structure at 40° 30’N, *Geophys. J. Int.*, **103**, 509–531.
- Whitmarsh, R.B., Pinheiro, L.M., Miles, P.R., Recq, M. & Sibuet, J.-C., 1993. Thin crust at the western Iberia ocean-continent transition and ophiolites, *Tectonics*, **12**, 1230–1239.
- Whitmarsh, R.B., White, R.S., Horsefield, S.J., Sibuet, J.-C., Recq, M. & Louvel, V., 1996. The ocean-continent boundary off the western continental margin of Iberia: crustal structure of Galicia Bank, *J. Geophys. Res.*, **101**(B12), 28291–28314.
- Whitmarsh, R.B., Manaischal, G. & Minshull, T.A., 2001. Evolution of magma-poor continental margins from final rifting to seafloor spreading, *Nature*, **413**, 150–154.
- Wilson, P.G., Turner, J.P. & Westbrook, G.K., 2003. Structural architecture of the ocean-continent boundary at an oblique transform margin through deep-imaging seismic interpretation and gravity modeling: Equatorial Guinea, West Africa, *Tectonophysics*, **374**, 19–40.
- Wu, Y., Loudon, K.E., Funck, T., Jackson, H.R. & Dehler, S.A., 2006. Crustal structure of the central Nova Scotia margin off Eastern Canada, *Geophys. J. Int.*, **166**, 878–906.
- Zelt, C.A., 1999. Modelling strategies and model assessment for wide-angle seismic traveltimes data, *Geophys. J. Int.*, **139**, 183–204.
- Zelt, C.A. & Smith, R.B., 1992. Seismic traveltimes inversion for 2-D crustal velocity structure, *Geophys. J. Int.*, **108**, 16–34.